

# Relative Impact of Right Ventricular Electromechanical Dyssynchrony Versus Pulmonary Regurgitation on Right Ventricular Dysfunction and Exercise Intolerance in Patients After Repair of Tetralogy of Fallot

Joost Lumens, PhD; Chun-Po Steve Fan, PhD;\* John Walmsley, PhD;\* Deane Yim, MD;\* Cedric Manlihot, PhD; Andreea Dragulescu, MD; Lars Grosse-Wortmann, MD; Luc Mertens, MD, PhD; Frits W. Prinzen, PhD; Tammo Delhaas, MD, PhD; Mark K. Friedberg, MD

**Background**—The relative impact of right ventricular (RV) electromechanical dyssynchrony versus pulmonary regurgitation (PR) on exercise capacity and RV function after tetralogy of Fallot repair is unknown. We aimed to delineate the relative effects of these factors on RV function and exercise capacity.

**Methods and Results**—We retrospectively analyzed 81 children with tetralogy of Fallot repair using multivariable regression. Predictor parameters were electrocardiographic QRS duration reflecting electromechanical dyssynchrony and PR severity by cardiac magnetic resonance. The outcome parameters were exercise capacity (percentage predicted peak oxygen consumption) and cardiac magnetic resonance ejection fraction (RV ejection fraction). To understand the relative effects of RV dyssynchrony versus PR on exercise capacity and RV function, virtual patient simulations were performed using a closed-loop cardiovascular system model (CircAdapt), covering a wide spectrum of disease severity. Eighty-one patients with tetralogy of Fallot repair (median [interquartile range {IQR}] age, 14.48 [11.55–15.91] years) were analyzed. All had prolonged QRS duration (median [IQR], 144 [123–152] ms), at least moderate PR (median [IQR], 40% [29%–48%]), reduced exercise capacity (median [IQR], 79% [68%–92%] predicted peak oxygen consumption), and reduced RV ejection fraction (median [IQR], 48% [44%–52%]). Longer QRS duration, more than PR, was associated with lower oxygen consumption and lower RV ejection fraction. In a multivariable regression analysis, oxygen consumption decreased with both increasing QRS duration and PR severity. CircAdapt modeling showed that RV dyssynchrony exerts a stronger limiting effect on exercise capacity and on RV ejection fraction than does PR, regardless of contractile function.

**Conclusions**—In both patient data and computer simulations, RV dyssynchrony, more than PR, appears to be associated with reduced exercise capacity and RV systolic dysfunction in patients after TOF repair. (*J Am Heart Assoc.* 2019;8:e010903. DOI: 10.1161/JAHA.118.010903)

**Key Words:** computer-based model • pulmonary regurgitation • right ventricular dysfunction • right ventricular dyssynchrony • tetralogy of Fallot • volume overload

Surgically repaired tetralogy of Fallot (rTOF) is the most prevalent cyanotic congenital heart disease. Although surgery in infancy has led to improved life expectancy and quality of life, residual lesions that result from surgical repair are common. These impact right ventricular (RV) size and

function and affect symptoms, exercise capacity, and long-term outcomes.<sup>1–4</sup>

There are multiple, often coexisting, reasons for progressive RV dysfunction in rTOF.<sup>3</sup> Among these, long-term volume loading resulting from chronic pulmonary regurgitation (PR) is

From the Division of Cardiology, Labatt Family Heart Centre, and Department of Paediatrics, Hospital for Sick Children and University of Toronto, Toronto, Ontario, Canada (C.-P.S.F., D.Y., C.M., A.D., L.G.-W., L.M., M.K.F.); Departments of Biomedical Engineering (J.L., J.W., T.D.) and Physiology (F.W.P.), Cardiovascular Research Institute Maastricht, Maastricht University, Maastricht, the Netherlands; and IHU LIRYC, Electrophysiology and Heart Modeling Institute, Fondation Bordeaux Université, Pessac, France (J.L.).

Accompanying Data S1 and Figures S1 through S5 are available at <https://www.ahajournals.org/doi/suppl/10.1161/JAHA.118.010903>

\*Dr Fan, Dr Walmsley, and Dr Yim contributed equally to this work.

**Correspondence to:** Mark K. Friedberg, MD, Division of Cardiology, The Labatt Family Heart Centre, The Hospital for Sick Children, 555 University Ave, Toronto, Ontario, Canada M5G 1X8. E-mail: [mark.friedberg@sickkids.ca](mailto:mark.friedberg@sickkids.ca)

Received September 11, 2018; accepted November 29, 2018.

© 2019 The Authors. Published on behalf of the American Heart Association, Inc., by Wiley. This is an open access article under the terms of the Creative Commons Attribution-NonCommercial-NoDerivs License, which permits use and distribution in any medium, provided the original work is properly cited, the use is non-commercial and no modifications or adaptations are made.

## Clinical Perspective

### What Is New?

- A significant proportion of patients with repaired tetralogy of Fallot have electromechanical dyssynchrony, which may substantially impact right ventricular function and exercise capacity more than the severity of pulmonary regurgitation.

### What Are the Clinical Implications?

- Many patients with tetralogy of Fallot repair and right ventricular dysfunction may benefit from cardiac resynchronization therapy.
- Addressing right ventricular electromechanical dyssynchrony may become a central therapeutic goal in repaired tetralogy of Fallot, in addition to, or independently of, pulmonary valve replacement.

thought to cause progressive RV dilation and dysfunction.<sup>2,5,6</sup> Consequently, several studies and guideline documents recommend replacing the pulmonary valve in patients with symptoms or in severely dilated RVs before development of irreversible RV remodeling.<sup>7</sup> The current indications and timing for pulmonary valve replacement (PVR) remain controversial and continue to be actively debated. Current practice in many centers includes replacing the pulmonary valve in asymptomatic patients, when the RV is enlarged beyond an end-diastolic volume of 150 to 170 mL/m<sup>2</sup> or an end-systolic volume of >90 mL/m<sup>2</sup>.<sup>7</sup> Although PVR leads to decreased RV volumes and subjective improvement in many patients, there is no conclusive evidence to show that it improves key clinical outcomes, such as exercise capacity, RV systolic function, and mortality.<sup>8,9</sup> Therefore, other factors may be important contributors to the progressive RV dysfunction commonly observed in this population.

Among the possible other causative factors for RV dysfunction, electromechanical abnormalities have been shown to be important.<sup>10,11</sup> After surgical rTOF, >90% of patients develop right bundle branch block (RBBB), and a prolonged QRS duration has been recognized as a major risk factor for ventricular arrhythmia and mortality.<sup>11</sup> We described that RBBB-induced electromechanical dyssynchrony is associated with RV dysfunction.<sup>12</sup> Accordingly, resynchronizing the dysfunctional RV could improve its hemodynamics, work, and efficiency.<sup>13</sup> However, the relative contribution of electromechanical dyssynchrony versus PR on RV function and exercise capacity is currently unknown. This knowledge gap is highly relevant because it is likely to influence patient management in terms of deciding between PVR and cardiac resynchronization therapy. Resynchronization of the dysfunctional subpulmonary RV in rTOF is not yet

routine therapy, but may be helpful in a portion of patients in whom RV electromechanical dyssynchrony underlies RV dysfunction and reduced exercise capacity.<sup>14,15</sup> Consequently, the aim of this study was to investigate the relative influence of PR versus electromechanical dyssynchrony on RV function and exercise capacity in rTOF. We hypothesized that electromechanical dyssynchrony is more strongly associated with RV dysfunction and exercise intolerance than PR.

## Methods

### Study Design

The data, analytic methods, and study materials will not be made available to other researchers for purposes of reproducing the results or replicating the procedure. To address the above research question, we used a dual approach using statistical analysis of patient data followed by computer modeling. We performed a clinically based, retrospective, cross-sectional statistical analysis of 81 children who had undergone surgical rTOF in early childhood to explore how QRS duration and PR are related to exercise capacity and RV function. We then performed virtual patient simulations covering a wide spectrum of disease severity to generate hypotheses about the relative mechanistic effect of RV dyssynchrony versus PR on exercise capacity and RV systolic function under tightly controlled and standardized circumstances. For this step, we used the CircAdapt model of the human heart and circulation, which has been shown to contribute to physiological understanding of both RV function and electromechanical dyssynchrony.<sup>16–18</sup>

### Study Population for the Clinical Analysis

We performed a retrospective cross-sectional analysis of data from patients whose data were collected between January 2007 and December 2014. The study was approved by the institutional research ethics board of the Hospital for Sick Children (Toronto, Ontario, Canada). Patients provided informed consent. A departmental database was used to screen for eligible patients (aged <18 years) after rTOF who had cardiac magnetic resonance (CMR) imaging. Patients who had a primary diagnosis of an atrioventricular septal defect with TOF or with more than minor (potentially hemodynamically significant) residual intracardiac shunts were excluded. Furthermore, to obtain a relatively homogeneous cohort in terms of volume loading as the predominant lesion, we excluded patients with moderate or severe RV outflow tract obstruction, defined as a Doppler-echocardiography outflow gradient >40 mm Hg,<sup>19</sup> within 6 months of CMR. Likewise, to avoid the major confounder of pacing-induced dyssynchrony, patients with active pacemakers were excluded. Because patients with rTOF/absent pulmonary

valve face the same clinical issues, and the influence of PR versus RBBB-dyssynchrony is relevant to this population, we included these patients in the analysis.

## Cardiac Magnetic Resonance

CMR was used to quantify RV volumes, RV ejection fraction (RVEF), and PR. CMR was performed on a 1.5-Tesla scanner (“Avanto”; Siemens Medical Systems, Erlangen, Germany). The clinical protocol included short-axis cine imaging for quantification of biventricular volumes and ejection fractions, as well as main pulmonary artery phase contrast flow velocity mapping for estimation of the PR volume and fraction. Ventricular volumes, mass, and flow quantification were performed using commercially available software (QMass Version 7.6 and QFlow Version 5.6; Medis Medical Imaging Systems, Leiden, the Netherlands).

## Clinical Parameters

Demographic and clinical data were collected from the medical record. Patients had cardiopulmonary exercise testing and a 12-lead body surface ECG within 6 months of CMR. Cardiopulmonary exercise testing was performed using a modified Bruce protocol. Peak oxygen consumption ( $VO_2$ ) and the percentage of predicted peak  $VO_2$  were recorded. The duration of the QRS complex was considered to be the continuous electrocardiographic parameter reflecting RV electromechanical dyssynchrony because all patients had an RBBB configuration on the ECG.

## Outcomes

The outcome variables were peak  $VO_2$ , which we also expressed as percentage of predicted  $VO_2$  (as commonly done in clinical practice), and RVEF, evaluated by CMR, as a measure of RV global systolic function.  $VO_2$  was normalized according to published data.<sup>20</sup> We also analyzed the relationship of PR and RBBB to RV end-systolic and end-diastolic volumes indexed to body surface area as parameters of RV remodeling.

## Independent Variables

QRS duration and PR fraction were the 2 independent variables of interest. Age, sex, body surface area, and heart rate (HR) were considered as covariates.

## Statistical Analyses

### Descriptive analysis

Continuous variables were summarized in terms of median and interquartile range; dichotomous variables were

summarized by frequencies and proportions. We also assessed correlations between QRS duration, PR fraction, and the outcome variables of interest using Spearman’s correlation. The 95% CIs of correlation coefficients were constructed using Fisher’s z-transformation.

### Multivariable regression analysis

The association between QRS duration, PR fraction, and peak  $VO_2$  was modeled using multivariable linear regression. The nonlinear association between an outcome variable and QRS duration and PR fraction was quantified using restricted cubic splines. The models included interactions between QRS duration and PR fraction, but these were restricted to linear-linear and linear-nonlinear interactions because of the limited sample size. Two regression models (namely, unadjusted and covariate-adjusted models) were used to examine the associations. The unadjusted models included only the independent variables of interest (QRS duration and PR fraction), whereas the adjusted model further included the aforementioned clinical covariates.

The proportion of missing values in all variables considered in the study varied between 1% and 20%. After the recommendation by Harrell,<sup>21</sup> 20 imputed data sets were constructed using a flexible additive regression spline model. Missing values in continuous variables were then imputed using predictive mean matching.<sup>21</sup> The final regression models were obtained by applying Rubin’s rules to combine the regression results across multiply imputed data sets. Diagnostic assessment of the final model was performed by inspecting residual plots.

We used heat maps to summarize predicted outcomes with respect to the independent variables of interest using both unadjusted and adjusted models. The estimated regression equations for the heat maps are included in the Appendix. Furthermore, the association was also adjusted for age, sex, body surface area, and HR. The association plots were created with average values for continuous covariates and for male sex. All analyses were conducted using R v3.4.1 with the rms package.

## Virtual Patient Simulations

### Reference rTOF simulation

The CircAdapt model is a closed-loop cardiovascular system model featuring contractile atria and ventricles, and lumped representations of the systemic and pulmonary circulations, separated by the 4 cardiac valves.<sup>22–24</sup> Structural adaptation to changes in hemodynamic loading can be simulated by varying the structure of the cardiovascular system (ie, mass, size, and passive stiffness of cardiac and vascular walls) through physiological adaptation rules.<sup>25</sup> For this study, resting conditions were taken to be a cardiac output (CO) of

5.4 L/min with an HR of 76 beats per minute, being the average values measured in the patient cohort with rTOF. The CO of 5.4 L/min is the effective systemic blood flow, which equals the output of the left ventricle, because the aortic and mitral valves are assumed to be competent. Mean arterial pressure was allowed to stabilize at 92 mm Hg through changes in systemic vascular resistance and circulating blood volume in all simulations. Two reference simulations were used in this study, one with healthy RV myocardium (the default CircAdapt model) and one with right atrial (RA) and RV myocardial dysfunction. The latter was created by reducing the RV and RA myocardial contractility to 50% of the healthy value, so that RVEF was in the range measured in the patient cohort with rTOF (44%–52%, Table 1), given a simulated PR fraction of 40% (ie, the median value of the patient cohort, Table 1). RA dysfunction was induced because the RA has been shown to be dysfunctional in association with RV dysfunction in rTOF.<sup>26,27</sup> Varying combinations of both PR and RV electromechanical dyssynchrony were then imposed on these 2 reference simulations, as described below, yielding 2 sets of 100 rTOF simulations. For each simulation, RVEF was quantified as the change in RV volume during systole divided by end-diastolic volume, as in the patients.

### Simulating PR

CircAdapt treats flow across the valve as being unsteady and nonviscous with a nonlinear flow profile. The Bernoulli equation is used to relate flow velocity and valve area to pressure decrease across the valve, with inertial effects on acceleration and deceleration attributable to blood mass included. In the standard CircAdapt model, the pulmonary valve begins to close once pulmonary arterial pressure exceeds RV pressure, with the valve's effective regurgitant orifice area being 0 cm<sup>2</sup> when the

valve is closed, preventing backward flow. Valvular regurgitation can be simulated in the CircAdapt model by setting the effective regurgitant orifice area to be nonzero, mimicking a hole in the valve through which retrograde flow can occur when pulmonary arterial pressure exceeds RV pressure (Figure S1). Retrograde flow uses the same equations as forward flow. Computational details are provided in the Appendix. In this study, the effective opening area of the pulmonary valve was 4.7 cm<sup>2</sup>. We used 10 effective regurgitant orifice areas ranging from 0 cm<sup>2</sup> (no PR) up to 2.25 cm<sup>2</sup> (severe PR) in steps of 0.25 cm<sup>2</sup>.

### Simulating electromechanical dyssynchrony

Electromechanical dyssynchrony was introduced into the RV of the CircAdapt model by dividing the RV free wall into 5 equally sized segments that can mechanically interact both with one another and with the left ventricular (LV) free wall and septum.<sup>24</sup> This method has previously been shown to produce realistic simulations of the dyssynchronously activated heart for both LV and RV stresses and strains as well as system-level hemodynamics.<sup>17,28</sup> Dispersion in onset of contraction (ie, sarcomeric force generation) within these RV free wall segments was introduced to simulate varying degrees of RBBB by delaying their activation relative to the LV free wall and septum. One RV segment was activated simultaneously with the LV, and the remaining 4 RV segments were activated at 25%, 50%, 75%, and 100% of the maximum delay in the RV free wall (Figure S2). Nine different maximum delays were used to simulate varying severities of RBBB, ranging from synchronous contraction (no RV delay) to severe contractile dyssynchrony (180-ms delay in the latest activated RV segment), in steps of 20 ms.

**Modeling exercise capacity.** Exercise can be simulated in CircAdapt by simultaneously increasing HR and CO. Exercise levels are achieved while increasing the circulating blood volume in the cardiovascular system, with mean arterial pressure maintained at 92 mm Hg through changes in systemic vascular resistance (Data S1). We hypothesized that increased central venous pressure (ie, mean vena cava pressure) is a limiting factor for the cardiovascular system's ability to perform exercise. To quantify exercise capacity and allow comparison between simulations, we assumed that it is impossible to perform exercise when mean pressure in the vena cava exceeds 25 mm Hg. This threshold was chosen because it is significantly in excess of the 15-mm Hg RA pressure reported by Stickland et al at near-peak exercise.<sup>29</sup> Sensitivity of results was tested against other pressure thresholds. For each of the virtual rTOF patient simulations described above, CO and HR were gradually increased from rest until the predefined threshold pressure was reached, with exercise capacity defined to be this threshold-reaching CO (CO<sub>max-exc</sub>). We used a fixed HR-CO relationship from the literature to determine the HR for a given CO (Figure S3).

**Table 1.** Clinical Characteristics of the Patient Cohort

Clinical Characteristic	N	Value*
Age, y	81	14.48 (11.55–15.91)
Sex	81	
Female		34 (42)
Male		47 (58)
Height, cm	76	155.0 (143.4–166.0)
Weight, kg	76	47.0 (34.8–66.0)
Body surface area, m <sup>2</sup>	79	1.46 (1.19–1.69)
Heart rate at CMR, bpm	80	76 (68–85)
QRS duration, ms	72	144 (123–152)
Pulmonary regurgitation fraction, %	76	40 (29–48)
Time between repair and CMR, y	75	13.0 (10.6–15.1)

bpm indicates beats per minute; CMR, cardiac magnetic resonance.

\*Values are given as median (interquartile range) or number (percentage).

## Results

### Clinical Cohort

Eighty-one patients with rTOF at a median (interquartile range) age of 14.48 (11.55–15.91) years were analyzed. The average age at time of repair was  $0.95 \pm 0.78$  years. Their clinical characteristics are shown in Table 1. All patients had prolonged QRS in an RBBB pattern and moderate PR (Table 1). The median time between cardiopulmonary exercise testing and CMR was 1.9 months. ECG and CMR were done on the same day in most patients.

The outcome variables of interest are presented in Table 2. Patients with rTOF had overall mildly to moderately reduced exercise capacity and mildly reduced RVEF.

### Association Between QRS Duration and PR on Exercise Capacity

Figure 1 shows the predicted peak  $VO_2$  without and with covariate adjustment in this patient cohort. In both heat maps, especially in that unadjusted for covariates, the association of prolonged QRS duration with predicted peak  $VO_2$  appeared to be stronger than that of PR severity. That is, moving from left to right on the heat map (increasing QRS duration) is, on average, associated with a lower peak  $VO_2$ ; however, moving from bottom to top on the heat map (increasing PR fraction) is not substantially associated with peak  $VO_2$ . Nonetheless, other factors likely impact exercise capacity because the heat maps also show a wide distribution of, for example, a  $VO_2$  of 40 mL/kg per minute. This distribution is likely also impacted by the relatively few patients available for analysis.

Figure 2 shows the statistically predicted RVEF with QRS duration and PR with and without covariate adjustment. The patterns with and without covariate adjustment were similar. As described above for peak  $VO_2$ , in both heat maps the association of progressively increasing QRS duration on RVEF is stronger than that of PR severity in both heat maps. That is, moving from left to right on the heat map (increasing QRS duration) is associated with a lower RVEF; however, moving from bottom to top on the heat map (increasing PR fraction) does not substantially impact RVEF.

**Table 2.** Outcome Variables Summarized as Medians and IQRs

Clinical Characteristics	N	Median (IQR)
Peak $VO_2$ , mL/min per $m^2$	65	35.0 (29.0–41.8)
Predicted peak $VO_2$ , %	65	79 (68–92)
RV ejection fraction, %	80	48 (44–52)
Cardiac index, L/min per $m^2$	79	3.67 (3.28–4.22)

IQR indicates interquartile range; RV, right ventricle;  $VO_2$ , oxygen consumption.

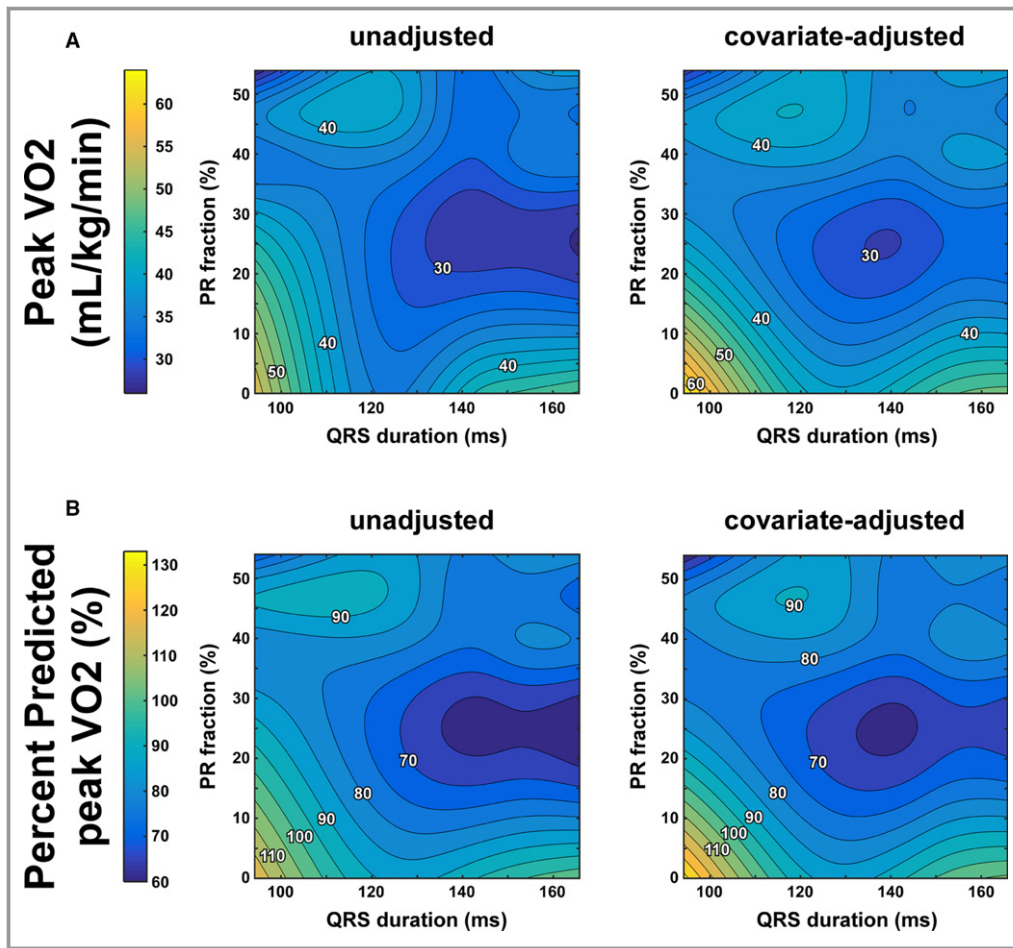
### Pairwise Correlation Analyses

Figure 3 shows the pairwise correlations between QRS duration, PR fraction, and the outcome variables of interest. There was a moderate negative correlation between QRS duration and RVEF such that a longer QRS duration was associated with a lower RVEF ( $r = -0.56$ ,  $P < 0.001$ ). There was no significant pairwise correlation between QRS duration and peak  $VO_2$  ( $r = -0.19$ ,  $r = 0.135$ ). PR fraction did not correlate at all with RVEF or peak  $VO_2$  ( $P > 0.5$ ).

### Virtual Patient Simulation Study

#### Effect on CO as a measure of exercise capacity

Figure 4 enables direct comparison of the simulated effects of PR versus RV dyssynchrony on exercise capacity in the virtual patient cohorts with rTOF with normal and decreased myocardial contractility (Figure 4A and 4B, respectively). The upper half of this figure illustrates how central venous pressure increases with CO during exercise in 4 representative virtual patients (ie, 1 without both PR and RV dyssynchrony [gray line], 1 with RV dyssynchrony alone [red line], 1 with PR alone [blue line], and 1 with both PR and RV dyssynchrony [purple line]). The lower half of the figure presents continuous heat maps of exercise capacity ( $CO_{\max\text{-exc}}$ ) as a function of RV dyssynchrony and PR, with the 4 representative virtual patients marked by circles. In general, these data suggest that RV dyssynchrony exerts a stronger limiting effect on exercise capacity than PR, regardless of myocardial contractile function. RV dyssynchrony alone (red line) was associated with a leftward shift of the central venous pressure–CO curve, with central venous pressure reaching the exercise-limiting threshold value at 30% lower CO than the virtual patient without PR and RV dyssynchrony and normal contractility (Figure 4A). Conversely, PR alone (blue line) had less effect on exercise capacity, with  $CO_{\max\text{-exc}}$  being only 5% lower than the virtual patient without PR and RV dyssynchrony and normal contractility. The limiting effect of PR and RV dyssynchrony on exercise capacity was additive, with  $CO_{\max\text{-exc}}$  being decreased by 36% in the virtual patient with both right heart pathological conditions, but normal contractility. RV contractile dysfunction had a profound exercise-limiting effect because the 50% right heart decrease in contractility lowered  $CO_{\max\text{-exc}}$  by 25% in the absence of PR and RV dyssynchrony (gray lines in Figure 4A versus Figure 4B). In the virtual patients with contractile dysfunction (Figure 4B), the relative effects on exercise capacity of RV dyssynchrony alone (27% decrease of  $CO_{\max\text{-exc}}$ ), PR alone (12% decrease of  $CO_{\max\text{-exc}}$ ), and both pathological conditions combined (36% decrease of  $CO_{\max\text{-exc}}$ ) were similar to those observed in the virtual patients with normal contractility. Different central venous pressure thresholds produced quantitatively similar



**Figure 1.** Predicted exercise capacity as function of right ventricular (RV) dyssynchrony and pulmonary regurgitation (PR) in the clinical patient cohort with tetralogy of Fallot repair. Exercise capacity is represented by peak oxygen consumption ( $\text{VO}_2$ ) (Panel A), whereas QRS duration is taken as a surrogate of RV dyssynchrony. Predicted peak  $\text{VO}_2$  values (Panel B) are presented without (left panel) as well as with (right panel) adjustment for covariates.

relationships between exercise capacity, PR, and RBBB, demonstrating that the relationship is insensitive to the choice of threshold (Figures S4 and S5).

#### Effect on RV Global Systolic Function and Remodeling

The effects of PR versus RV dyssynchrony on RV volumes and global systolic function (ie, RVEF) are shown in Figure 5.

RVEF decreased with increasing RV dyssynchrony, but increased with PR severity, regardless of myocardial contractile function (Figure 5A and 5B). An RV activation delay of 120 ms alone reduced RVEF from 63% to 54% in the virtual patients with normal contractility and from 53% to 42% in those with RV and RA contractile dysfunction. In contrast, PR alone increased RVEF to supranormal or normal values in the virtual patients with normal and decreased contractility, respectively (Figure 5A and 5B).

PR and RV delay cause a similar increase in RV end-diastolic volume (Figure 5C and 5D), whereas RV end-systolic

volume increased more strongly with RV activation delay than with PR (Figure 5E and 5F). The latter is most likely because of the fact that RV dyssynchrony impairs RV systolic function, whereas PR does so less.

#### Relation of hemodynamics with PR or RBBB to exercise level

Figure 6 illustrates how PR fraction and RV  $\text{dp}/\text{dt}$  (change in pressure over time) maximum change ( $\text{dp}/\text{dt}_{\text{max}}$ ) with increasing exercise intensity in the same sample of 4 representative virtual patients. Figure 6A (top) shows that, with normal contractility, the PR fraction decreases as the exercise level increases in the virtual patient with PR only (blue line). The additional presence of RV dyssynchrony (purple line) does not significantly affect this reduction. Figure 6A (bottom) shows that the increase in RV  $\text{dp}/\text{dt}_{\text{max}}$  during exercise is similar in the PR-only case (blue line) and the no pathological condition case (gray line). Figure 6B shows that the results are qualitatively

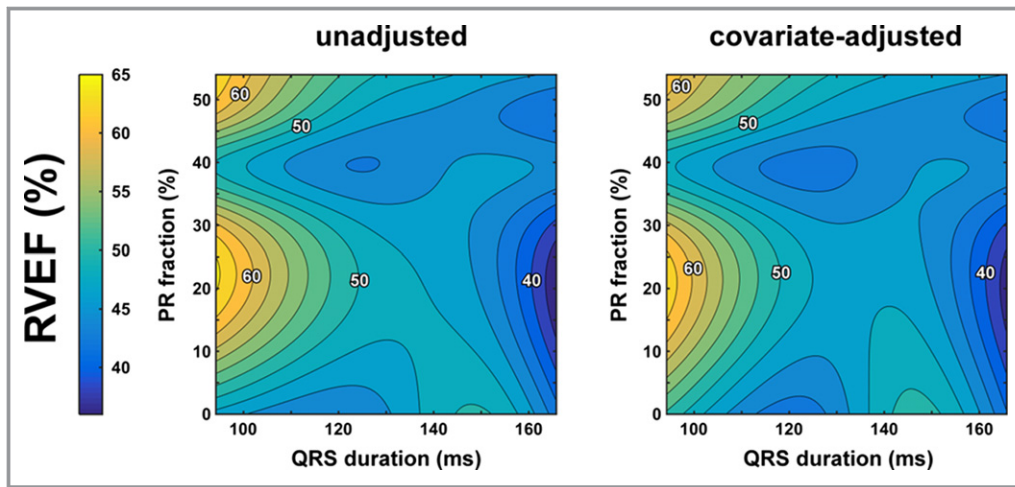


**Figure 2.** Predicted resting right ventricular (RV) systolic function as function of RV dyssynchrony and pulmonary regurgitation (PR) in the clinical patient cohort with tetralogy of Fallot repair. RV systolic function is represented by RV ejection fraction (RVEF), whereas QRS duration is taken as a surrogate of RV dyssynchrony. Predicted resting RVEF values are presented without (left panel) as well as with (right panel) adjustment for covariates.

similar when RV contractile dysfunction is present, although the RV  $dp/dt_{max}$  is reduced and lower values of  $CO_{max-exc}$  are reached. These simulation results strongly suggest that the relatively small compromising effect of PR on exercise capacity is attributable to a diminishing PR fraction as HR increases with exercise intensity, while systolic RV function is maintained. In contrast, the virtual patients with dyssynchrony (Figure 6A, red and purple lines) show reduced RV  $dp/dt_{max}$  at rest in comparison with the no pathological condition and PR-only simulations. Furthermore, increasing exercise level results in less increase in RV  $dp/dt_{max}$  in the virtual patients with dyssynchrony compared with the ones without, causing the difference in systolic RV function between the 2 to increase with exercise intensity. This effect was further exacerbated by the presence of RV contractile dysfunction, which severely reduces the increase in RV  $dp/dt_{max}$  when dyssynchrony is present (Figure 6B). Therefore, in contrast to the effects of PR alone, the limiting effect of RV dyssynchrony on RV contractility is large at all levels of exercise and worsens as exercise level increases.

## Discussion

In this unique exploratory study incorporating clinical observation and computer modeling, we compared the pathophysiological contributions and associations of RV volume loading from PR versus those of RBBB-dyssynchrony on RV (dys)function and exercise capacity in patients after rTOF. The integrative modeling approach was instrumental in relating cardiac function to exercise capacity in a complex population with coexisting and incompletely characterized pathological conditions (ie, RBBB and PR). The mechanistic nature of this

approach suggests that our results may have applicability beyond rTOF and that the relation between bundle-branch block and exercise capacity in other patient populations merits further investigation.

The main result of this study is that dyssynchrony in patients with rTOF, reflected by the duration of the QRS complex, appears to be substantially more associated with reduced exercise capacity and RV systolic dysfunction compared with PR in these patients. Computer modeling leads us to hypothesize that the association of prolonged QRS in an RBBB pattern with reduced exercise capacity observed in the patients is a direct mechanistic consequence of RV dyssynchrony. Alleviation of RV volume loading by PVR is currently a central therapeutic goal of rTOF management; yet, although RV dyssynchrony is common in this population, cardiac resynchronization therapy is not commonly considered and is not a routine therapy. Thus, our results may have important implications for future investigations into the relative merits of cardiac resynchronization therapy and/or PVR for improving outcomes in patients with rTOF.

## Effect of PR on RV Function and Exercise Capacity

Previous studies have shown reduced RV function in rTOF, which is most commonly attributed to volume loading and RV remodeling from PR.<sup>30</sup> Consequently, PVR has been recommended as the primary treatment for RV dilatation, remodeling, and/or dysfunction in this setting.<sup>7</sup>

However, previous studies have shown varying results when investigating the relationship between reduction of PR

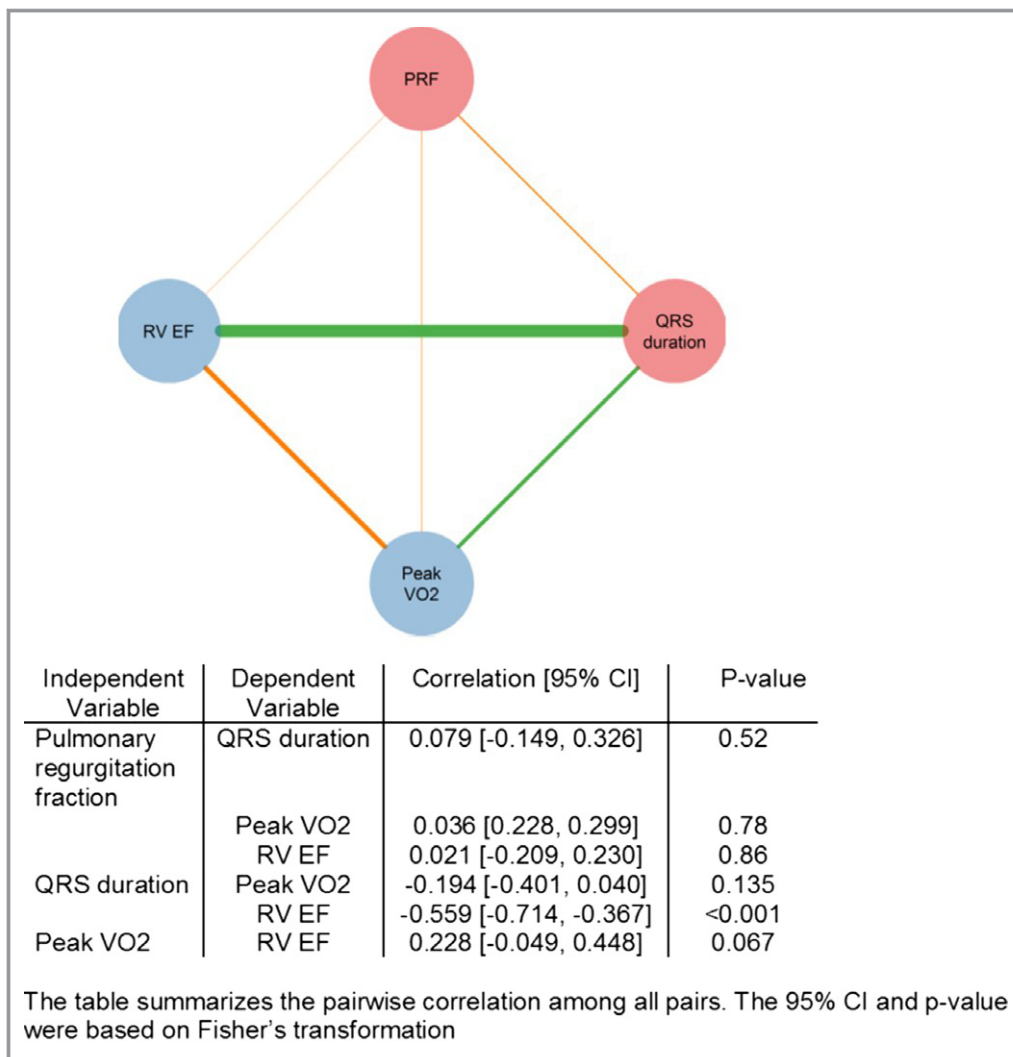


**Figure 3.** Univariable correlations of the outcome parameters in the clinical cohort. Circles and edges represented variables and pairwise Spearman's correlation, respectively. Red circles represent independent variables (ie, pulmonary regurgitation and QRS duration); blue circles represent the outcome variables. Orange edges show a positive correlation between 2 variables; green edges show a negative one. The thicker an edge is, the stronger the correlation is. RVEF indicates right ventricular ejection fraction; VO<sub>2</sub>, oxygen consumption. PRF indicates pulmonary regurgitant fraction.

through PVR and RV function. Our group recently found in a preoperative pediatric TOF cohort that RV end-diastolic volumes correlated with RV myocardial strain and that those patients with larger preoperative RV volumes had lower RV strain postoperatively.<sup>31</sup> We also found that after PVR, an increase in global RV strain beyond preoperative values may suggest positive RV remodeling and adaptation. These results differ from other studies in which 6 months after surgical PVR, strain did not improve.<sup>31,32</sup> Eyskens et al found a moderate correlation between the PR percentage and RV strain.<sup>33</sup> In contrast, Frigiola et al found that RV strain was reduced to a similar degree regardless of the severity of PR.<sup>30</sup> When evaluating global function, most studies have not found an improvement in RVEF after PVR,<sup>9</sup> which is consistent with our

current results that the severity of PR was not associated with RVEF. Although some studies have found improvement in exercise capacity after PVR, those patients had predominantly pressure-loaded RVs and only mild PR.<sup>34</sup> Our findings are consistent with empirical findings that PVR does not lead to improved global RV function or exercise capacity in the chronically volume-loaded RV.<sup>19</sup> Because RV dysfunction is a risk factor for death, our results are also consistent with studies in which alleviation of PR by PVR was not associated with a reduced rate of death or sustained VT.<sup>9,35</sup> In fact, one recent multicenter study suggested that there may even be a detrimental effect for inappropriate PVR in subjects not meeting consensus criteria for PVR.<sup>35</sup> RV remodeling, beyond RV volume per se, likely determines RV function and response

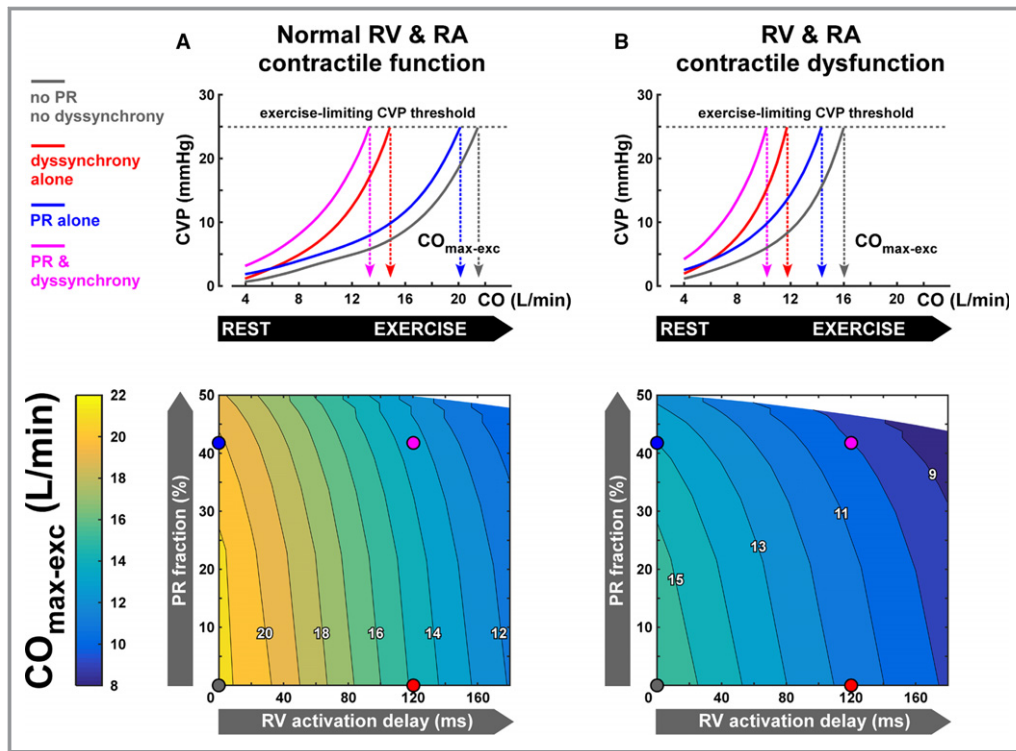


**Figure 4.** Exercise capacity as function of right ventricular (RV) dyssynchrony and pulmonary regurgitation (PR) in the virtual patient cohorts with tetralogy of Fallot repair (rTOF) and normal (A) and decreased (B) contractile function of the RV and right atrial (RA) myocardium. The upper panels show how central venous pressure (CVP) increases with CO during exercise in 4 representative virtual patients with rTOF. Those virtual patients are marked by circles in the heat plots showing continuous effects of RV dyssynchrony and PR on exercise capacity. Simulated exercise capacity is defined as the virtual patient's cardiac output ( $CO_{max-exc}$ ) associated with the exercise-limiting CVP threshold. In general, RV dyssynchrony and contractile dysfunction are more limiting for exercise capacity than PR.

to PVR; and recent studies have suggested that RV end-systolic volume, possibly representing systolic function, is associated with adverse outcomes.<sup>35</sup> The question remains whether a more aggressive approach and early prevention of PR, before the development of irreversible RV remodeling and dysfunction, ultimately improves exercise tolerance and outcomes.<sup>7</sup>

### Effect of Dyssynchrony on RV Function and Exercise Capacity

Electrophysiological markers have long been identified as risk factors for adverse outcomes in rTOF. In landmark studies, Gatzoulis et al identified a prolonged QRS duration as a major risk factor for sudden death in patients with rTOF, although the more recent INDICATOR (International Multicenter TOF Registry) cohort study failed to confirm this result.<sup>2,11,36</sup> Although some studies have not found a link between RV dyssynchrony and clinical outcomes, they used relatively nonspecific markers of mechanical dispersion.<sup>28,37,38</sup> Recently, QRS duration >160 ms, in addition to RV volumes,

has been found to predict adverse outcomes.<sup>35</sup> We recently identified specific mechanical patterns of RBBB-induced mechanical dyssynchrony associated with RV inefficiency and dysfunction<sup>12</sup>; and others have subsequently shown that acutely resynchronizing the dyssynchronous subpulmonary RV can increase its function and mechanical efficiency.<sup>13</sup> Moreover, we previously found that increased mechanical dyssynchrony, which is a consequence of RBBB-induced QRS prolongation, correlates with decreased exercise capacity in rTOF,<sup>39</sup> and that mechanical dyssynchrony worsens during exercise, possibly explaining reduced exercise capacity in this population through a negative feedback loop.<sup>40</sup> Similarly, a large magnetic resonance study recently found increased mechanical delay, in association with prolonged QRS duration, that was associated with lower exercise peak  $VO_2$  and worse RV and LV global function.<sup>41</sup> Those results are concordant with the results of the current study, in which we found that a longer QRS duration is associated with decreased RV global function and worse exercise tolerance, suggesting that narrowing the QRS via pacing may be an effective treatment to improve exercise capacity. Moreover, our modeling results

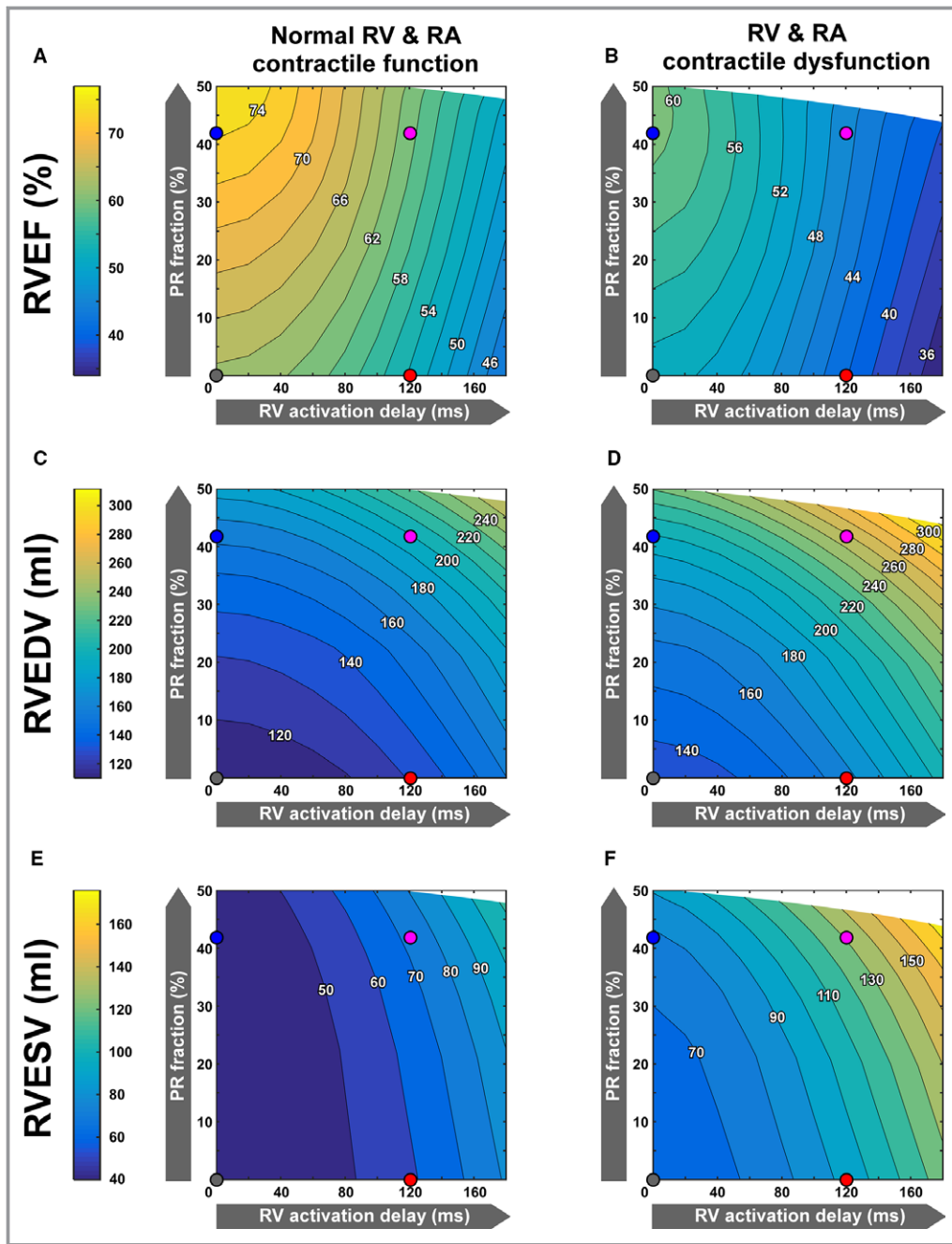


**Figure 5.** Resting right ventricular (RV) systolic function (A and B) and end-diastolic (C and D) and end-systolic (E and F) volumes as a function of RV dyssynchrony and pulmonary regurgitation (PR) in the virtual patient cohorts with tetralogy of Fallot repair and normal (A, C, and E) and decreased (B, D, and F) contractile function of the RV and right atrial (RA) myocardium. Simulated RV systolic function is represented by the virtual patient’s RV ejection fraction (RVEF). RVEF decreased with increasing RV dyssynchrony, but increased with PR severity, regardless of myocardial contractile function (A and B). PR and RV delay causes a similar increase in RV end-diastolic volume (RVEDV; C and D), whereas RV end-systolic volume (RVESV) increased more strongly with RV activation delay than with PR (E and F).

suggest that, when RV contractility is reduced, critical thresholds that would correspond to severe exercise intolerance are reached much more quickly when QRS duration is prolonged. This finding suggests that the effect of a prolonged

QRS on exercise capacity is particularly important when RV contractility is decreased. These simulations also suggest that underlying myocardial failure (ie, difference between A and B in Figure 4) may be an important confounder in the patient

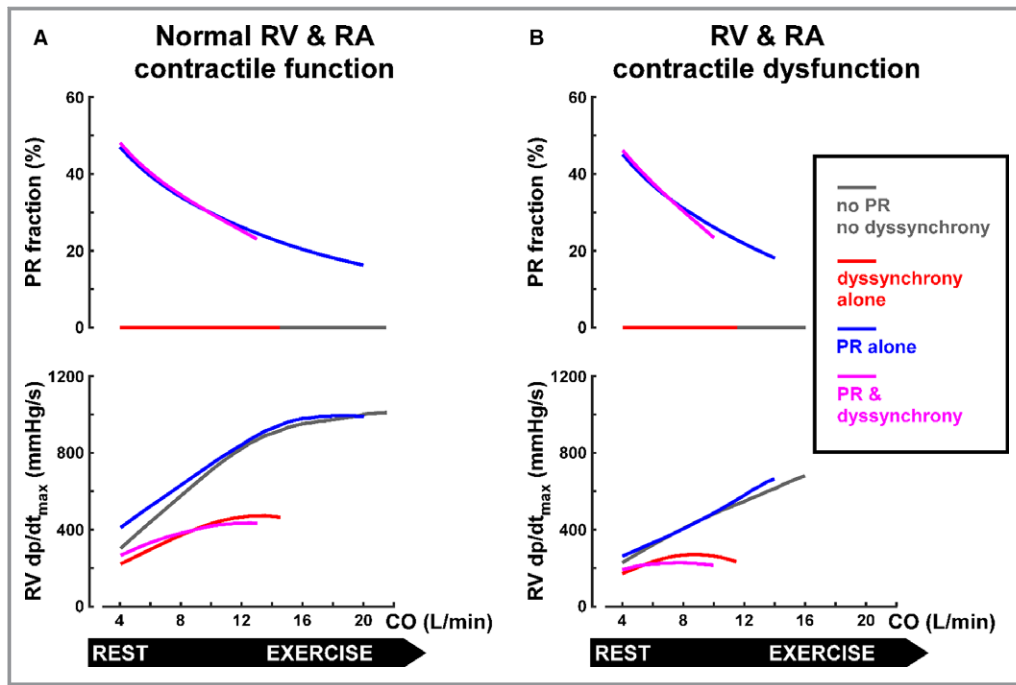


**Figure 6.** Valvular regurgitation (top) and global right ventricular (RV) contractility (bottom) as functions of exercise level in virtual patients with tetralogy of Fallot repair (rTOF) and normal (A) and decreased (B) contractile function of the RV and right atrial (RA) myocardium. The 4 representative virtual patients with rTOF are the same as in Figures 4 and 5. Lines are plotted until maximal cardiac output during exercise ( $CO_{\max\text{-exc}}$ ) is reached. The pathological consequences of pulmonary regurgitation (PR), as quantified by PR fraction, decrease with exercise level (top), whereas RV dyssynchrony reduces RV global contractility and this effect becomes more pronounced as exercise level increases.  $dp/dt_{\max}$  indicates maximal change in pressure over time.

data. These simulations strongly suggest that interindividual differences in myocardial contractile strength/failure are one of the confounders that we do not measure/quantify in the patients and may therefore cause some of the variability in the patient heat plots for peak  $VO_2$ .

The clinical translation of our findings may not be straightforward because at least one study found that RV pacing may not narrow the QRS complex, and consequently does not lead to hemodynamic improvement.<sup>42</sup> However, the same group found, both in experimental models and in a few adults with rTOF, that cardiac resynchronization therapy via biventricular pacing improved RV and LV function by improving electromechanical dyssynchrony, as manifested by a reduced QRS duration and electrical mapping-activation studies.<sup>43</sup> In these animals and in patients, PR was left untreated. These results are consistent with our findings that QRS duration, more than PR fraction, is associated with RV dysfunction and consequently exercise intolerance. Moreover, a recent study has demonstrated that short-term RV free wall pacing with fusion and native activation can both shorten the QRS complex and improve hemodynamic parameters in children with rTOF, at least within 24 hours of surgery.<sup>44</sup>

Gatzoulis et al found that QRS duration was related to RV dilatation, and one study found a reduction in QRS duration

after PVR.<sup>36</sup> This is in contrast to our current results, stemming from both modeling and observational data. It is also in contrast to our prior studies in which QRS duration was not associated with RV size.<sup>39</sup> The differences in results may relate to the different ages of the cohorts and differences in era and surgical management because we do not exclude the idea that in dilated and scarred ventricles, more common in older patients managed in previous years, distal conduction disease may progress and potentially contribute to progressive dyssynchrony.

### Agreement Between Computer Modeling and Empirical Data

Predictions afforded by modeling could not and cannot be entirely validated. Moreover, specifically in our study, the cross-sectional retrospective observational design cannot validate the modeling results. Nonetheless, as an exploratory study, the clinical observations and empirical statistical associations were consistent with the predicted effects from computer modeling. Furthermore, the computer model allowed us to hypothesize a mechanistic explanation for our clinical findings. The combined approach of using computer modeling alongside clinical observations has been

contributory in LV pathological conditions,<sup>18,28</sup> but is much less characterized for the RV.<sup>17</sup> Our group has combined computer modeling with clinical observations to understand mechanisms of RV dysfunction and to assist with clinical decision making in other diseases.<sup>45,46</sup> As a future perspective, the combination of modeling with clinical data, such as imaging, may be useful to understand which patients with rTOF have mechanical dyssynchrony amenable to resynchronization and are, hence, most likely to benefit from electrical rather than, or possibly together with, hemodynamic therapy.<sup>12,17</sup>

## Limitations

In the clinical cohort, the range of PR was relatively narrow and the number of patients with severe PR was limited. This limits our ability to corroborate the computer modeling of severe PR. Likewise, by design, we excluded patients with moderate to severe RV outflow tract obstruction. Therefore, our results may not apply to patients with mixed pressure and volume loading, and this should be studied in the future. We could not evaluate the “hard” clinical outcomes of sustained ventricular tachycardia or death because these are uncommon in children and cannot be modeled in a computer model based on hemodynamics. Therefore, reduced exercise tolerance, the most prominent clinical outcome parameter in childhood and adolescence, was chosen as the independent clinical outcome. It would be pertinent to study regional wall motion abnormalities by echocardiography as the mechanical correlate of RBBB dyssynchrony that determines RV dysfunction and exercise capacity.<sup>12,40</sup> This will be the topic of future investigations, and in this initial study, we chose to focus on QRS duration because it is the primary, and most quantifiable and clinically applicable, parameter of RBBB dyssynchrony. In the future, it would also be interesting to further model effects of regional RV dysfunction on clinical outcomes.

## Conclusion

In conclusion, in both patient data and computer simulations, RV dyssynchrony, more than PR, appears to be associated with reduced exercise capacity and RV systolic dysfunction in patients after rTOF. Computer modeling allowed us to hypothesize that this association between QRS prolongation and reduced exercise capacity may be causative. On the basis of previous literature and our current results, both PR and RV dyssynchrony appear to impact RV function and exercise tolerance; and the question in the individual patient is what is the balance between these factors. Our results suggest that in many cases, RV resynchronization might be helpful after rTOF. These results have important implications for future

investigations and subsequently the management goals of this important population.

## Sources of Funding

Dr Lumens acknowledges support from the Dr Dekker Program of the Dutch Heart Foundation (grant 2015T082) and the Netherlands Organization for Scientific Research (NWO-ZonMw, VIDI grant 016.176.340).

## Disclosures

Dr Lumens has received funding from Medtronic Bakken Research Center for consulting services. The remaining authors have no disclosures to report.

## References

- Orwat S, Diller GP, Kempny A, Radke R, Peters B, Kuhne T, Boethig D, Gutberlet M, Dubowy KO, Beerbaum P, Sarikouch S, Baumgartner H; German Competence Network for Congenital Heart Defects Investigators. Myocardial deformation parameters predict outcome in patients with repaired tetralogy of Fallot. *Heart*. 2016;102:209–215.
- Valente AM, Gauvreau K, Assenza GE, Babu-Narayan SV, Schreier J, Gatzoulis MA, Groenink M, Inuzuka R, Kilner PJ, Koyak Z, Landzberg MJ, Mulder B, Powell AJ, Wald R, Geva T. Contemporary predictors of death and sustained ventricular tachycardia in patients with repaired tetralogy of Fallot enrolled in the INDICATOR cohort. *Heart*. 2014;100:247–253.
- Geva T. Repaired tetralogy of Fallot: the roles of cardiovascular magnetic resonance in evaluating pathophysiology and for pulmonary valve replacement decision support. *J Cardiovasc Magn Reson*. 2011;13:9.
- Larios G, Friedberg MK. Imaging in repaired tetralogy of Fallot with a focus on recent advances in echocardiography. *Curr Opin Cardiol*. 2017;32:490–502.
- Knauth AL, Gauvreau K, Powell AJ, Landzberg MJ, Walsh EP, Lock JE, del Nido PJ, Geva T. Ventricular size and function assessed by cardiac MRI predict major adverse clinical outcomes late after tetralogy of Fallot repair. *Heart*. 2008;94:211–216.
- Geva T, Sandweiss BM, Gauvreau K, Lock JE, Powell AJ. Factors associated with impaired clinical status in long-term survivors of tetralogy of Fallot predict evaluated by magnetic resonance imaging. *J Am Coll Cardiol*. 2004;43:1068–1074.
- Tretter JT, Friedberg MK, Wald RM, McElhinney DB. Defining and refining indications for transcatheter pulmonary valve replacement in patients with repaired tetralogy of Fallot: contributions from anatomical and functional imaging. *Int J Cardiol*. 2016;221:916–925.
- Geva T, Gauvreau K, Powell AJ, Cecchin F, Rhodes J, Geva J, del Nido P. Randomized trial of pulmonary valve replacement with and without right ventricular remodeling surgery. *Circulation*. 2010;122(suppl):S201–S208.
- Harrild DM, Berul CI, Cecchin F, Geva T, Gauvreau K, Pigula F, Walsh EP. Pulmonary valve replacement in tetralogy of Fallot: impact on survival and ventricular tachycardia. *Circulation*. 2009;119:445–451.
- Vogel M, Sponring J, Cullen S, Deanfield JE, Redington AN. Regional wall motion and abnormalities of electrical depolarization and repolarization in patients after surgical repair of tetralogy of Fallot. *Circulation*. 2001;103:1669–1673.
- Gatzoulis MA, Balaji S, Webber SA, Siu SC, Hokanson JS, Poile C, Rosenthal M, Nakazawa M, Moller JH, Gillette PC, Webb GD, Redington AN. Risk factors for arrhythmia and sudden cardiac death late after repair of tetralogy of Fallot: a multicentre study. *Lancet*. 2000;356:975–981.
- Hui W, Slorach C, Dragulescu A, Mertens L, Bijns B, Friedberg MK. Mechanisms of right ventricular electromechanical dyssynchrony and mechanical inefficiency in children after repair of tetralogy of Fallot. *Circ Cardiovasc Imaging*. 2014;7:610–618.
- Janousek J, Kovanda J, Lozek M, Tomek V, Vojtovic P, Gebauer R, Kubus P, Krejcir M, Lumens J, Delhaas T, Prinzen F. Pulmonary right ventricular resynchronization in congenital heart disease: acute improvement in right

- ventricular mechanics and contraction efficiency. *Circ Cardiovasc Imaging*. 2017;10:e0006424.
14. Kubus P, Materna O, Tax P, Tomek V, Janousek J. Successful permanent resynchronization for failing right ventricle after repair of tetralogy of Fallot. *Circulation*. 2014;130:e186–e190.
  15. Friedberg MK. Another step in the right direction: resynchronizing the dyssynchronous right ventricle improves its efficiency and function. *Circ Cardiovasc Imaging*. 2017;10:e006905.
  16. Lumens J, Delhaas T. Cardiovascular modeling in pulmonary arterial hypertension: focus on mechanisms and treatment of right heart failure using the CircAdapt model. *Am J Cardiol*. 2012;110(suppl):39S–48S.
  17. Walmsley J, van Everdingen W, Cramer MJ, Prinzen FW, Delhaas T, Lumens J. Combining computer modelling and cardiac imaging to understand right ventricular pump function. *Cardiovasc Res*. 2017;113:1486–1498.
  18. Lumens J, Ploux S, Strik M, Gorcsan J III, Cochet H, Derval N, Strom M, Ramanathan C, Ritter P, Haissaguerre M, Jais P, Arts T, Delhaas T, Prinzen FW, Bordachar P. Comparative electromechanical and hemodynamic effects of left ventricular and biventricular pacing in dyssynchronous heart failure: electrical resynchronization versus left-right ventricular interaction. *J Am Coll Cardiol*. 2013;62:2395–2403.
  19. Coats L, Khambadkone S, Derrick G, Hughes M, Jones R, Mist B, Pellerin D, Marek J, Deanfield JE, Bonhoeffer P, Taylor AM. Physiological consequences of percutaneous pulmonary valve implantation: the different behaviour of volume- and pressure-overloaded ventricles. *Eur Heart J*. 2007;28:1886–1893.
  20. Washington RL, van Gundy JC, Cohen C, Sondheimer HM, Wolfe RR. Normal aerobic and anaerobic exercise data for North American school-age children. *J Pediatr*. 1988;112:223–233.
  21. Harrell F. *Regression Modeling Strategies: With Applications to Linear Models, Logistic and Ordinal Regression and Survival Analysis*. 2nd ed. Basel, Switzerland: Springer International Publishing; 2015.
  22. Lumens J, Delhaas T, Kirn B, Arts T. Three-wall segment (TriSeg) model describing mechanics and hemodynamics of ventricular interaction. *Ann Biomed Eng*. 2009;37:2234–2255.
  23. Arts T, Delhaas T, Bovendeerd P, Verbeek X, Prinzen FW. Adaptation to mechanical load determines shape and properties of heart and circulation: the CircAdapt model. *Am J Physiol Heart Circ Physiol*. 2005;288:H1943–H1954.
  24. Walmsley J, Arts T, Derval N, Bordachar P, Cochet H, Ploux S, Prinzen FW, Delhaas T, Lumens J. Fast simulation of mechanical heterogeneity in the electrically asynchronous heart using the MultiPatch module. *PLoS Comput Biol*. 2015;11:e1004284.
  25. Arts T, Lumens J, Kroon W, Delhaas T. Control of whole heart geometry by intramyocardial mechano-feedback: a model study. *PLoS Comput Biol*. 2012;8:e1002369.
  26. Kutty S, Shang Q, Joseph N, Kowalick JT, Schuster A, Steinmetz M, Danford DA, Beerbaum P, Sarikouch S. Abnormal right atrial performance in repaired tetralogy of Fallot: a CMR feature tracking analysis. *Int J Cardiol*. 2017;248:136–142.
  27. Riesenkampff E, Al-Wakeel N, Kropf S, Stamm C, Alexi-Meskishvili V, Berger F, Kuehne T. Surgery impacts right atrial function in tetralogy of Fallot. *J Thorac Cardiovasc Surg*. 2014;147:1306–1311.
  28. Lumens J, Tayal B, Walmsley J, Delgado-Montero A, Huntjens PR, Schwartzman D, Althouse AD, Delhaas T, Prinzen FW, Gorcsan J III. Differentiating electromechanical from non-electrical substrates of mechanical discoordination to identify responders to cardiac resynchronization therapy. *Circ Cardiovasc Imaging*. 2015;8:e003744.
  29. Stickland MK, Welsh RC, Petersen SR, Tyberg JV, Anderson WD, Jones RL, Taylor DA, Bouffard M, Haykowsky MJ. Does fitness level modulate the cardiovascular hemodynamic response to exercise? *J Appl Physiol*. 2006;100:1895–1901.
  30. Frigiola A, Redington AN, Cullen S, Vogel M. Pulmonary regurgitation is an important determinant of right ventricular contractile dysfunction in patients with surgically repaired tetralogy of Fallot. *Circulation*. 2004;110(suppl 1):II153–II157.
  31. Yim D, Mertens L, Morgan CT, Friedberg MK, Grosse-Wortmann L, Dragulescu A. Impact of surgical pulmonary valve replacement on ventricular mechanics in children with repaired tetralogy of Fallot. *Int J Cardiovasc Imaging*. 2017;33:711–720.
  32. Knirsch W, Dodge-Khatami A, Kadner A, Kretschmar O, Steiner J, Bottler P, Kececioglu D, Harpes P, Valsangiacomo Buechel ER. Assessment of myocardial function in pediatric patients with operated tetralogy of Fallot: preliminary results with 2D strain echocardiography. *Pediatr Cardiol*. 2008;29:718–725.
  33. Eyskens B, Brown SC, Claus P, Dymarkowski S, Gewillig M, Bogaert J, Mertens L. The influence of pulmonary regurgitation on regional right ventricular function in children after surgical repair of tetralogy of Fallot. *Eur J Echocardiogr*. 2010;11:341–345.
  34. Batra AS, McElhinney DB, Wang W, Zakheim R, Garofano RP, Daniels C, Yung D, Cooper DM, Rhodes J. Cardiopulmonary exercise function among patients undergoing transcatheter pulmonary valve implantation in the US Melody valve investigational trial. *Am Heart J*. 2012;163:280–287.
  35. Bokma JP, Geva T, Sleeper LA, Babu Narayan SV, Wald R, Hickey K, Jansen K, Wassall R, Lu M, Gatzoulis MA, Mulder BJ, Valente AM. A propensity score-adjusted analysis of clinical outcomes after pulmonary valve replacement in tetralogy of Fallot. *Heart*. 2018;104:738–744.
  36. Gatzoulis MA, Till JA, Somerville J, Redington AN. Mechano-electrical interaction in tetralogy of Fallot: QRS prolongation relates to right ventricular size and predicts malignant ventricular arrhythmias and sudden death. *Circulation*. 1995;92:231–237.
  37. Moon TJ, Choueier N, Geva T, Valente AM, Gauvreau K, Harrild DM. Relation of biventricular strain and dyssynchrony in repaired tetralogy of fallot measured by cardiac magnetic resonance to death and sustained ventricular tachycardia. *Am J Cardiol*. 2015;115:676–680.
  38. Jing L, Wehner GJ, Suever JD, Charnigo RJ, Alhadad S, Stearns E, Mojsenjo K, Haggerty CM, Hickey K, Valente AM, Mulder BJ, Powell AJ, Fornwalt BK. Left and right ventricular dyssynchrony and strains from cardiovascular magnetic resonance feature tracking do not predict deterioration of ventricular function in patients with repaired tetralogy of Fallot. *J Cardiovasc Magn Reson*. 2016;18:49.
  39. Friedberg MK, Fernandes FP, Roche SL, Slorach C, Grosse-Wortmann L, Manlhiot C, Fackoury C, McCrindle BW, Mertens L, Kantor PF. Relation of right ventricular mechanics to exercise tolerance in children after tetralogy of Fallot repair. *Am Heart J*. 2013;165:551–557.
  40. Roche SL, Grosse-Wortmann L, Redington AN, Slorach C, Smith G, Kantor PF, Friedberg MK. Exercise induces biventricular mechanical dyssynchrony in children with repaired tetralogy of Fallot. *Heart*. 2010;96:2010–2015.
  41. Kalaitzidis P, Orwat S, Kempny A, Robert R, Peters B, Sarikouch S, Beerbaum P, Baumgartner H, Diller GP; Competence Network for Congenital Heart Defects, DZHK (German Center for Cardiovascular Research). Biventricular dyssynchrony on cardiac magnetic resonance imaging and its correlation with myocardial deformation, ventricular function and objective exercise capacity in patients with repaired tetralogy of Fallot. *Int J Cardiol*. 2018;264:53–57.
  42. Bordachar P, Iriart X, Chabaneix J, Sacher F, Lafitte S, Jais P, Haissaguerre M, Clementy J, Dos Santos P, Thambo JB. Presence of ventricular dyssynchrony and haemodynamic impact of right ventricular pacing in adults with repaired tetralogy of Fallot and right bundle branch block. *Europace*. 2008;10:967–971.
  43. Thambo JB, Dos Santos P, De Guillebon M, Roubertie F, Labrousse L, Sacher F, Iriart X, Lafitte S, Ploux S, Jais P, Roques X, Haissaguerre M, Ritter P, Clementy J, Narayan SM, Bordachar P. Biventricular stimulation improves right and left ventricular function after tetralogy of Fallot repair: acute animal and clinical studies. *Heart Rhythm*. 2010;7:344–350.
  44. Vojtovic P, Kucera F, Kubus P, Gebauer R, Matejka T, Tlaskal T, Lozek M, Kovanda J, Janousek J. Acute right ventricular resynchronization improves haemodynamics in children after surgical repair of tetralogy of Fallot. *Europace*. 2018;20:323–328.
  45. Palau-Caballero G, Walmsley J, Van Empel V, Lumens J, Delhaas T. Why septal motion is a marker of right ventricular failure in pulmonary arterial hypertension: mechanistic analysis using a computer model. *Am J Physiol Heart Circ Physiol*. 2017;312:H691–H700.
  46. van Everdingen WM, Walmsley J, Cramer MJ, van Hagen I, De Boeck BWL, Meine M, Delhaas T, Doevendans PA, Prinzen FW, Lumens J, Leenders GE. Echocardiographic prediction of cardiac resynchronization therapy response requires analysis of both mechanical dyssynchrony and right ventricular function: a combined analysis of patient data and computer simulations. *J Am Soc Echocardiogr*. 2017;30:1012–1020.e2.

# **SUPPLEMENTAL MATERIAL**

## Data S1. Statistical methods

We used the following to denote an indicator function and a ramp function.

$[c] = 1$  if subject is in group  $c$ , 0 otherwise;  $(x)_+ = x$  if  $x > 0$ , 0 otherwise

We also denoted QRS duration and pulmonary regurgitation fraction by QRS and PRF, respectively.

### 1 Unadjusted regression equations

The estimated unadjusted regression equations are

$$\begin{aligned} E(\text{Peak VO}_2) = & 147.8166 - 0.97761 \text{QRS} - 1.86186 \text{PRF} + \\ & 0.00041 (\text{QRS} - 96)_+^3 - 0.00195 (\text{QRS} - 128)_+^3 + 0.00307 (\text{QRS} - 144)_+^3 - \\ & 0.00159 (\text{QRS} - 152)_+^3 + 5.14479 \times 10^{-5} (\text{QRS} - 170)_+^3 - \\ & 0.00179 (\text{PRF} - 5)_+^3 + 0.02694 (\text{PRF} - 31)_+^3 - 0.08738 (\text{PRF} - 40)_+^3 + \\ & 0.09876 (\text{PRF} - 47)_+^3 - 0.03653 (\text{PRF} - 54)_+^3 + \\ & \text{QRS} \left\{ 0.01582 \text{PRF} + 1.61583 \times 10^{-5} (\text{PRF} - 5)_+^3 - 0.00022 (\text{PRF} - 31)_+^3 + \right. \\ & \quad \left. 0.00066 (\text{PRF} - 40)_+^3 - 0.00072 (\text{PRF} - 47)_+^3 + 0.00026 (\text{PRF} - 54)_+^3 \right\} + \\ & \text{PRF} \left\{ 7.08476 \times 10^{-6} (\text{QRS} - 96)_+^3 - 9.44531 \times 10^{-5} (\text{QRS} - 128)_+^3 + \right. \\ & \quad \left. 0.00029 (\text{QRS} - 144)_+^3 - 0.00023 (\text{QRS} - 152)_+^3 + 2.44597 \times 10^{-5} (\text{QRS} - 170)_+^3 \right\} \end{aligned}$$

$$\begin{aligned} E(\text{Percent predicted VO}_2) = & 246.9357 - 1.35484 \text{QRS} - 2.662 \text{PRF} + \\ & 0.00045 (\text{QRS} - 96)_+^3 - 0.00159 (\text{QRS} - 128)_+^3 + 0.00128 (\text{QRS} - 144)_+^3 + \\ & 6.66333 \times 10^{-6} (\text{QRS} - 152)_+^3 - 0.00014 (\text{QRS} - 170)_+^3 - \\ & 0.0026 (\text{PRF} - 5)_+^3 + 0.04865 (\text{PRF} - 31)_+^3 - 0.17193 (\text{PRF} - 40)_+^3 + \\ & 0.2022 (\text{PRF} - 47)_+^3 - 0.07633 (\text{PRF} - 54)_+^3 + \\ & \text{QRS} \left\{ 0.01664 \text{PRF} + 2.7652 \times 10^{-5} (\text{PRF} - 5)_+^3 - 0.00042 (\text{PRF} - 31)_+^3 + \right. \\ & \quad \left. 0.00136 (\text{PRF} - 40)_+^3 - 0.00153 (\text{PRF} - 47)_+^3 + 0.00057 (\text{PRF} - 54)_+^3 \right\} + \\ & \text{PRF} \left\{ 1.21243 \times 10^{-5} (\text{QRS} - 96)_+^3 - 0.00018 (\text{QRS} - 128)_+^3 + 6 \times 10^{-4} (\text{QRS} - 144)_+^3 - \right. \\ & \quad \left. 0.00048 (\text{QRS} - 152)_+^3 + 5.70184 \times 10^{-5} (\text{QRS} - 170)_+^3 \right\} \end{aligned}$$

$$\begin{aligned} E(\text{RV EF}) = & 66.36041 - 0.20258 \text{QRS} + 3.15599 \text{PRF} + \\ & 0.00014 (\text{QRS} - 96)_+^3 - 0.00079 (\text{QRS} - 128)_+^3 + 4.70158 \times 10^{-5} (\text{QRS} - 144)_+^3 + \end{aligned}$$

$$\begin{aligned}
& 0.00117 (\text{QRS} - 152)_+^3 - 0.00058 (\text{QRS} - 170)_+^3 - \\
& 0.00347 (\text{PRF} - 5)_+^3 + 0.04447 (\text{PRF} - 31)_+^3 - 0.10589 (\text{PRF} - 40)_+^3 + \\
& 0.08992 (\text{PRF} - 47)_+^3 - 0.02504 (\text{PRF} - 54)_+^3 + \\
& \text{QRS} \left\{ -0.02244 \text{PRF} + 2.44557 \times 10^{-5} (\text{PRF} - 5)_+^3 - 0.00032 (\text{PRF} - 31)_+^3 + \right. \\
& \quad \left. 0.00077 (\text{PRF} - 40)_+^3 - 0.00067 (\text{PRF} - 47)_+^3 + 0.00019 (\text{PRF} - 54)_+^3 \right\} \\
& \text{PRF} \left\{ 1.07228 \times 10^{-5} (\text{QRS} - 96)_+^3 - 0.00014 (\text{QRS} - 128)_+^3 + 0.00034 (\text{QRS} - 144)_+^3 - \right. \\
& \quad \left. 0.00021 (\text{QRS} - 152)_+^3 - 1.42996 \times 10^{-6} (\text{QRS} - 170)_+^3 \right\}
\end{aligned}$$

## 2 Covariate-adjusted regression equations

The estimated covariate-adjusted regression equations are

$$\begin{aligned}
E(\text{Peak VO}_2) = & 174.2491 - 0.56777 \text{Age} - 4.9794 \text{BSA} + 4.23814 [\text{Male}] - \\
& 0.10510 \text{HR MRI} - 0.97461 \text{QRS} - 3.3355 \text{PRF} + \\
& 0.0003 (\text{QRS} - 96)_+^3 - 0.00092 (\text{QRS} - 128)_+^3 + 7.11016 \times 10^{-5} (\text{QRS} - 144)_+^3 + \\
& 0.00081 (\text{QRS} - 152)_+^3 - 0.00026 (\text{QRS} - 170)_+^3 - \\
& 0.00016 (\text{PRF} - 5)_+^3 + 0.01092 (\text{PRF} - 31)_+^3 - 0.05103 (\text{PRF} - 40)_+^3 + \\
& 0.06727 (\text{PRF} - 47)_+^3 - 0.027 (\text{PRF} - 54)_+^3 + \\
& \text{QRS} \left\{ 0.02432 \text{PRF} + 5.30983 \times 10^{-6} (\text{PRF} - 5)_+^3 - 0.00011 (\text{PRF} - 31)_+^3 + \right. \\
& \quad \left. 0.00042 (\text{PRF} - 40)_+^3 - 0.00052 (\text{PRF} - 47)_+^3 + 0.0002 (\text{PRF} - 54)_+^3 \right\} + \\
& \text{PRF} \left\{ 2.32814 \times 10^{-6} (\text{QRS} - 96)_+^3 - 4.8851 \times 10^{-5} (\text{QRS} - 128)_+^3 + 0.00019 (\text{QRS} - 144)_+^3 - \right. \\
& \quad \left. 0.00016 (\text{QRS} - 152)_+^3 + 2.43571 \times 10^{-5} (\text{QRS} - 170)_+^3 \right\}
\end{aligned}$$

$$\begin{aligned}
E(\text{Percent predicted VO}_2) = & 353.9556 - 1.49809 \text{Age} - 9.7086 \text{BSA} + 0.35758 [\text{Male}] - \\
& 0.187401 \text{HR MRI} - 1.84289 \text{QRS} - 6.46064 \text{PRF} + \\
& 0.00056 (\text{QRS} - 96)_+^3 - 0.00158 (\text{QRS} - 128)_+^3 - 0.00036 (\text{QRS} - 144)_+^3 + \\
& 0.00191 (\text{QRS} - 152)_+^3 - 0.00053 (\text{QRS} - 170)_+^3 - \\
& 0.00052 (\text{PRF} - 5)_+^3 + 0.02354 (\text{PRF} - 31)_+^3 - 0.10593 (\text{PRF} - 40)_+^3 + \\
& 0.13819 (\text{PRF} - 47)_+^3 - 0.05527 (\text{PRF} - 54)_+^3 + \\
& \text{QRS} \left\{ 0.0463 \text{PRF} + 1.29855 \times 10^{-5} (\text{PRF} - 5)_+^3 - 0.00024 (\text{PRF} - 31)_+^3 + \right. \\
& \quad \left. 0.00089 (\text{PRF} - 40)_+^3 - 0.00107 (\text{PRF} - 47)_+^3 + 0.00041 (\text{PRF} - 54)_+^3 \right\} + \\
& \text{PRF} \left\{ 5.69359 \times 10^{-6} (\text{QRS} - 96)_+^3 - 0.00011 (\text{QRS} - 128)_+^3 + 0.00039 (\text{QRS} - 144)_+^3 - \right.
\end{aligned}$$

$$0.00034 (\text{QRS} - 152)_+^3 + 4.85806 \times 10^{-5} (\text{QRS} - 170)_+^3 \}$$

$$\begin{aligned} E(\text{RV EF}) = & 115.4021 - 1.06927 \text{ Age} + 3.8795 \text{ BSA} - 0.74171[\text{Male}] - \\ & 0.123603 \text{ HR MRI} - 0.47508 \text{ QRS} + 1.89948 \text{ PRF} + \\ & 0.00026 (\text{QRS} - 96)_+^3 - 0.00149 (\text{QRS} - 128)_+^3 + 0.00158 (\text{QRS} - 144)_+^3 + \\ & 0.00013 (\text{QRS} - 152)_+^3 - 0.00048 (\text{QRS} - 170)_+^3 - \\ & 0.00299 (\text{PRF} - 5)_+^3 + 0.03969 (\text{PRF} - 31)_+^3 - 0.09509 (\text{PRF} - 40)_+^3 + \\ & 0.08067 (\text{PRF} - 47)_+^3 - 0.02229 (\text{PRF} - 54)_+^3 + \\ & \text{QRS} \left\{ -0.01212 \text{ PRF} + 2.10403 \times 10^{-5} (\text{PRF} - 5)_+^3 - 0.00028 (\text{PRF} - 31)_+^3 + \right. \\ & \quad \left. 0.00068 (\text{PRF} - 40)_+^3 - 0.00059 (\text{PRF} - 47)_+^3 + 0.00017 (\text{PRF} - 54)_+^3 \right\} + \\ & \text{PRF} \left\{ 9.22529 \times 10^{-6} (\text{QRS} - 96)_+^3 - 0.00012 (\text{QRS} - 128)_+^3 + 0.0003 (\text{QRS} - 144)_+^3 - \right. \\ & \quad \left. 0.00018 (\text{QRS} - 152)_+^3 - 1.55424 \times 10^{-6} (\text{QRS} - 170)_+^3 \right\} \end{aligned}$$

## Data S2. Supplemental Material: Computer modeling

### Supplementary Methods

#### *Valve module and Pulmonary Valve Regurgitation*

The valve module is used to simulate blood flow across any connection between two cavities or a cavity and a tube in the CircAdapt model where energy losses might occur. Cardiac valves connect cardiac cavities, representing atrio-ventricular valves, or connect cardiac cavities with large blood vessels, representing ventriculo-arterial valves. The valve module is also used to represent connections between veins and atria, or atrial and ventricular septal defects. The valve module consists of a narrow orifice whose area varies over time during a cardiac cycle. Assuming unsteady, incompressible and non-viscous laminar flow, and the influence of gravity being neglected, the Bernoulli equation for unsteady flow can be written as,

$$I \cdot \frac{dq}{dt} + \frac{1}{2} \rho \cdot (v_{dist}(t)^2 - v_{prox}(t)^2) + (p_{dist}(t) - p_{prox}(t)) = 0 \quad (1)$$

where  $\rho$  is blood density,  $I$  is the inertance of the valve, and  $dq/dt$  is the rate of change of blood flow across the valve. The blood flow velocities and pressures at the proximal and distal elements are  $v_{prox}(t)$  and  $p_{prox}(t)$ , and  $v_{dist}(t)$  and  $p_{dist}(t)$ , respectively (**Supplementary Figure 1**). By re-arranging **Eq. 1**, the pressure gradient ( $\Delta p(t) = p_{prox}(t) - p_{dist}$ ) can be expressed as,

$$\Delta p(t) = I \frac{dq}{dt} + \frac{1}{2} \rho \cdot (v_{dist}(t)^2 - v_{prox}(t)^2) \quad (2)$$

Since we assume that when blood flow passes a valve, there is no regain in pressure despite a decrease in velocity (i.e. energy is lost by means of friction or turbulence), **Eq. 2** can be re-arranged as,

$$\Delta p(t) = I \cdot \frac{dq_{valve}}{dt} + \frac{1}{2} \rho \cdot \begin{cases} v_{max}(t)^2 - v_{prox}(t)^2, & q_{valve}(t) \geq 0 \\ v_{dist}(t)^2 - v_{max}(t)^2, & q_{valve}(t) < 0 \end{cases} \quad (3)$$

The pressure gradient in **Eq. 3** is the sum of inertial effects, i.e., blood acceleration/deceleration because of blood mass (**Eq. 3**, right hand side, first term) and Bernoulli pressure loss effects (**Eq. 3**, right hand side, second term). Blood flow,  $q_{valve}(t)$ , across a valve is defined as forward flow ( $q_{valve}(t) \geq 0$ ) when it travels from the proximal into the distal element, and backward flow ( $q_{valve}(t) < 0$ ) in the opposite direction. In **Eq. 3**, the maximum velocity,  $v_{max}(t)$ , is:

$$v_{max}(t) = \max\{v_{prox}(t), v_{valve}(t), v_{dist}(t)\}. \quad (4)$$

Flow velocities  $v_{prox}(t)$ ,  $v_{valve}(t)$  and  $v_{dist}(t)$  are calculated as valve flow,  $q_{valve}(t)$ , divided by the cross-sectional area at the proximal element, valve and distal elements at time  $t$ , respectively. The effective orifice area (or cross-sectional area) of a valve at time  $t$ ,  $A_{valve}(t)$ , is determined by the pressure gradient. When the valve is open,  $A_{valve}(t) = A_{open}$ , and when it is closed,  $A_{valve}(t) = A_{leak}$ . The valve opens rapidly when the pressure gradient is positive ( $p_{dist}(t) < p_{prox}(t)$ ), allowing forward flow across the valve into the distal element. When the distal pressure is equal to the proximal pressure ( $p_{dist}(t) = p_{prox}(t)$ ), the valve starts closing. In the closing state, the pressure gradient is negative ( $p_{dist}(t) > p_{prox}(t)$ ), but a forward flow can briefly exist because of inertial effects (**Eq. 1**). A valve finally closes when the pressure gradient is negative and no forward flow remains. Note that in this study, a 'closed' valve allows retrograde flow to occur through the regurgitant orifice area as described in the main text, because  $A_{leak}$  can be non-zero.

The inertance of a tube  $I = \alpha \frac{\rho l}{A}$ , where  $l$  is the length of the tube and  $A$  is the cross sectional area.  $\alpha$  is a constant reflecting the non-linearity of the flow profile. CircAdapt uses  $\alpha = 3/2$ , representing a highly nonlinear flow through the valve (compare with  $\alpha=1$  for plug flow and  $\alpha = 4/3$  for Poiseuille flow). In CircAdapt, the inertance takes into account blood moving through the areas immediately proximal to the valve, and immediately distal to the valve (**Supplementary Figure 1**). Combining these effects gives a total expression for the inertance as

$$I = \frac{3}{2} \rho \left( \frac{l_{valve}}{A_{valve}} + \frac{1}{2} \left( \frac{1}{\sqrt{A_{prox}}} + \frac{1}{\sqrt{A_{dist}}} \right) \right) \quad (5)$$

Note, as stated before, that the valve module is used to connect any two cavities in the CircAdapt model where energy losses might occur, such as veins returning to the atria, or in case of an atrial or ventricular septal defect. In these cases, we define  $A_{leak} = A_{open}$ .

#### *Flow across the systemic and pulmonary circulations*

The CircAdapt model consists of a four-chamber heart connected to a closed loop cardiovascular system, with lumped pulmonary and systemic circulations (**Supplementary Figure 2, Panel A**). The systemic circulation is modelled as a vascular resistance connecting the aorta with the systemic veins. In CircAdapt, both the arterial and venous pressures vary with time, and the pressure difference

between the arteries and veins determines the flow across the systemic circulation at any point in time,  $t$ . The time-dependent flow across the systemic circulation  $q_{sys}(t)$  is assumed to relate with time-dependent pressure drop  $\Delta p_{sys}(t)$  as,

$$q_{sys}(t) = \frac{q_{sys,ref}}{\Delta p_{sys,ref}} \cdot \Delta p_{sys}(t) \quad (6)$$

where  $q_{sys,ref}$  is the reference circulating blood flow and  $\Delta p_{sys,ref}$  is the corresponding reference systemic pressure drop.  $\Delta p_{sys}(t) = p_{sys,art}(t) - p_{sys,ven}(t)$  is the difference between the pressure in the systemic arteries ( $p_{sys,art}(t)$ ) and the systemic veins ( $p_{sys,ven}(t)$ ) at each time point. By Ohm's law,  $\frac{q_{sys,ref}}{\Delta p_{sys,ref}}$  is the resistance of the systemic vasculature. In the CircAdapt model,  $q_{sys,ref}$  is always held constant, but  $\Delta p_{sys,ref}$  can be changed between cardiac cycles in the homeostatic control system described below. Hence, changing  $\Delta p_{sys,ref}$  changes the systemic resistance in CircAdapt. Intuitively,  $\Delta p_{sys,ref}$  can be seen as the pressure difference between the systemic arteries and systemic veins that would be required to generate a constant systemic flow of  $q_{sys,ref}$ . The relationship for the pulmonary circulation is similar to **Eq. 6**,

$$q_{pulm}(t) = \frac{q_{pulm,ref}}{\Delta p_{pulm,ref}^2} \cdot \Delta p_{pulm}(t)^2 \quad (7)$$

where  $q_{pulm,ref}$  is the reference pulmonary circulating blood flow and  $\Delta p_{pulm,ref}$  is the corresponding pulmonary pressure drop. The quadratic relationship in **Eq. 7** is based on measurements of pulmonary circulatory haemodynamics in dogs.<sup>11</sup> A description of the systemic and pulmonary circulation models, including the pressure-volume relationships in the major arteries and veins, can be found in Arts et al, *Mech Res Commun* 2011;42:15-21.

### *Pressure-flow regulation*

In CircAdapt, homeostatic pressure-flow regulation is used to maintain a target cardiac output ( $q_{sys,target}$ ) and target mean systemic arterial pressure ( $MAP_{target}$ ). In the current study,  $q_{sys,target}$  changes depending on the level of exercise. Note that  $q_{sys,target}$  is not necessarily the same as  $q_{sys,ref}$  in **Eq. 6** above. In CircAdapt, homeostatic pressure-flow regulation represents two physiological processes. Acutely, it represents the recruitment of pooled blood in the venous system into the circulating blood volume. In the longer term (for example when employed in simulations of heart failure, e.g.: Lumens et al, *Circ Cardiovasc Imaging* 2015;8:e003744), it represents the long-term action of the Renin-Angiotensin-Aldosterone system (RAAS) on fluid retention to maintain cardiac output. Both interpretations are

present in this study, with the former used in exercise and the latter used to maintain the baseline cardiac output.

When pressure-flow regulation is enabled, CircAdapt calculates at the end of each cardiac cycle the ratio between the current mean systemic arterial pressure over the cardiac cycle ( $MAP_{current} = \overline{p_{sys,art}(t)}$ ) and the target mean aortic pressure ( $MAP_{target}$ ) (**Supplementary Figure 2, red dot**). This ratio is then used to incrementally alter the systemic resistance through changes in  $\Delta p_{sys,ref}$  (**Eq. 6**), with the process repeated over repeated cardiac cycles until  $MAP_{current} = MAP_{target}$ . In this study, a  $MAP_{target}$  of 92mmHg was used. After each cardiac cycle, the new value of the constant  $\Delta p_{sys,ref}$ , which determines the systemic vascular resistance during the next cardiac cycle (**Eq. 6**), is calculated using:

$$\Delta p_{sys,ref,new} = \left( \frac{MAP_{target}}{MAP_{current}} \right)^\alpha \cdot \left( \frac{q_{sys,current}}{q_{sys,target}} \right)^\alpha \Delta p_{sys,ref,old} \quad (8)$$

Hence, the systemic vascular resistance will increase when MAP is too low, and decrease when systemic flow is too low.  $\alpha < 1$  is a damping factor that prevents oscillatory behaviour. Note that the pulmonary resistance remains unchanged.

To represent RAAS and/or recruitment of pooled blood, the circulating blood volume alters with the systemic vascular resistance. These processes are implemented by injecting or removing volume per cardiac cycle into the cardiac system from the systemic vascular bed, i.e. by altering the flow at the arrow highlighted in **Supplementary Figure 2 (Panel A, red arrow)**. The flow across the systemic circulation  $q(t)$  is calculated at each time point  $t$  in the cardiac cycle using **Eq. 6**. The flow entering the systemic veins  $q_{ven}(t)$  at each time point is then adjusted, so that

$$q_{ven}(t) = \left( \frac{MAP_{target}}{MAP_{current}} \right)^\alpha q(t) \quad (9)$$

Equivalently, **Eq. 9** can be seen as including an additional flow of magnitude  $\left( \left( \frac{MAP_{target}}{MAP_{current}} \right)^\alpha - 1 \right) q(t)$  into the flow exiting the systemic circulation into the systemic veins. Note that if  $MAP_{target} > MAP_{current}$ , then the additional flow is positive, analogous to recruitment of pooled blood into the circulation or fluid retention by RAAS. If  $MAP_{current} > MAP_{target}$  then this flow is negative and removes blood from the circulation, analogous to blood pooling in the veins or fluid excretion through RAAS.

### *Simulating Exercise*

The above method is used to simulate exercise by using an imposed cardiac output – heart rate relationship (**Supplemental Figure 3**). In this relationship, the heart rate is used to determine cycle length  $t_{\text{Cycle}}$ , which is an input to the model. In CircAdapt, cycle length determines the time period between onsets of right atrial contraction. The target cardiac output corresponding to that heart rate is set as  $q_{\text{sys,target}}$  in **Eq. 8** above, with  $MAP_{\text{target}}$  left unchanged at 92mmHg. The system is then allowed to stabilize until  $MAP_{\text{target}}$  and  $q_{\text{sys,target}}$  are reached.

To enable realistic simulation of exercise, the atrio-ventricular delay between right atrial activation and onset of ventricular activation (first activated segment in **Supplemental Figure 2**) has to shorten with decreasing cycle time, representing physiological PR interval shortening. CircAdapt sets the atrio-ventricular delay to be  $0.1765 \times t_{\text{Cycle}}$ .

Duration of myocardial contraction also shortens as the heart rate increases (i.e, cycle time decreases). CircAdapt uses a phenomenological model of myocardial contraction, described in detail in the supplemental material of Walmsley et al, PLoS Comput Biol 2015;11:e1004284. The rise time ( $\tau_R$ ), decay time ( $\tau_D$ ) and contraction duration ( $T_A$ ) all depend on the cycle length as follows,

$$\tau_R = T_R T_{Act} \quad (10)$$

$$\tau_D = T_D T_{Act} \quad (11)$$

$$T_A = (0.65 + 1.057 \lambda_{si}) T_{Act} \quad (12)$$

Where  $T_D$  and  $T_R$  are constants,  $\lambda_{si}$  is the extension of the contractile element, and

$$T_{Act} = 0.1 t_{\text{Cycle,rest}} + 0.4 t_{\text{Cycle}}, \quad (13)$$

where  $t_{\text{Cycle,Rest}}$  is the cycle time at rest.

### *Dyssynchronous Activation*

Dyssynchrony is simulated using the MultiPatch method as described by Walmsley et al. PLoS Comput Biol 2015;11:e1004284, to which the reader is referred for methodological details. This method allows ventricular walls to be broken up into ‘patches’ of tissue and thereby simulate regional differences in function. Wall tension is assumed to be equal in all patches within a wall, but properties such as activation time can vary between patches, giving rise to differences in stresses and strains between patches. In the current study, the right ventricular free wall was broken up into five patches with equal

volumes. Only activation time differs between patches; myocardial intrinsic contractility and stiffness are not altered. The right ventricular free wall also interacts with the septum and LV free wall through the right ventricular attachment points, where force balance is enforced. The reader is referred to Lumens et al. Ann Biomed Eng 2009;37:2234-2255 for methodological details on ventricular interaction.

#### Simulation Code

The code for the CircAdapt model used in this study is free to download at [www.circadapt.org](http://www.circadapt.org). This study is based on the version previously published by Walmsley et al., PLoS Comput Biol 2015;11:e1004284.

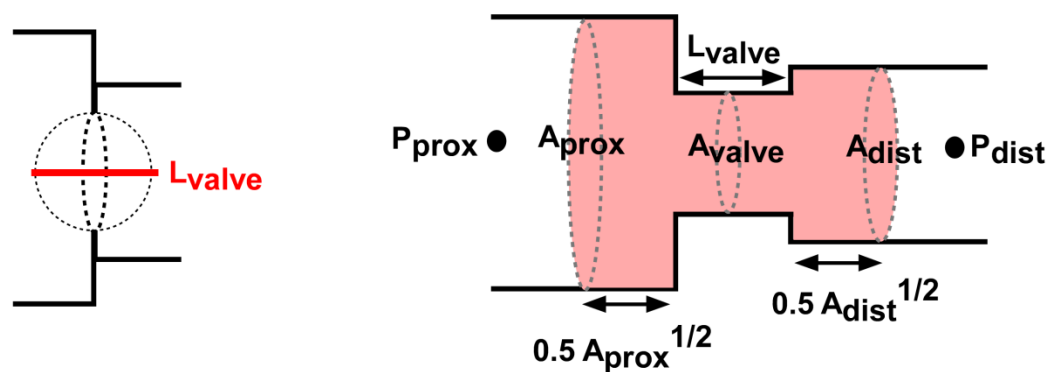


**Figure S1:** Definitions used in the text for the simulation of valvular function. The pink area indicates the total volume of blood considered in the inertance of the valve.

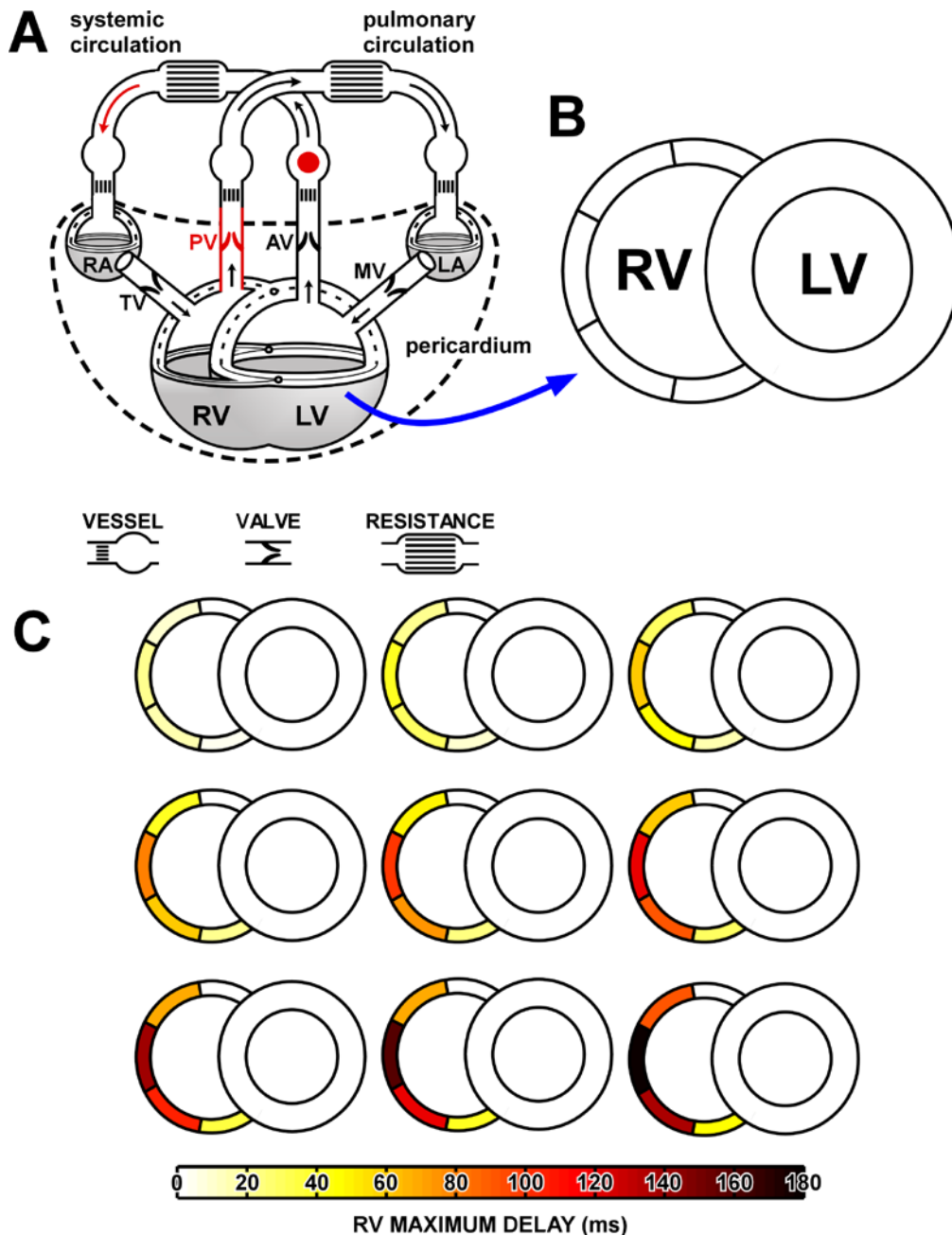


**Figure S2:** Panel A shows a schematic diagram of the CircAdapt model, modified from Lumens et al. *Ann Biomed Eng.* 2009;37(11):2234-55, with permission. Red has been used to highlight key parts of the model for this study referred to in the supplemental methods, being the pulmonary valve, pressure control in the aorta, and systemic venous return. Panel B shows a schematic of the ventricles in the synchronous case, with location in the model indicated by the blue arrow. Note that the LV is always synchronously activated in this study. Panel C shows the remaining nine activation patterns, with progressively increasing delay within the RV free wall. The colour bar indicates the magnitude of the delay in each segment. RV segments are activated at 0%, 25%, 50%, 75% and 100% of the latest RV activation time in each case.

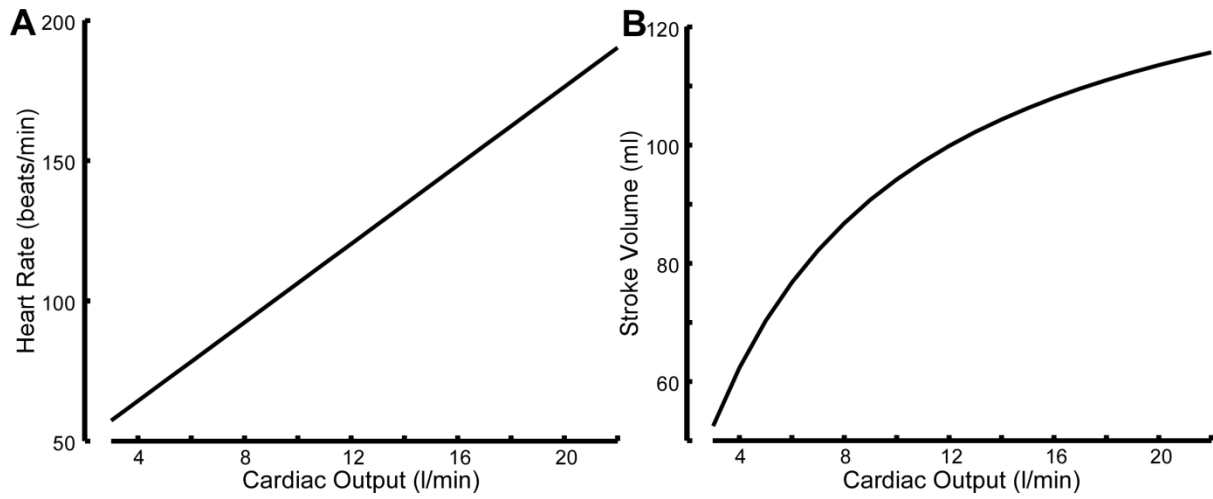


**Figure S3:** Heart rate – LV cardiac output relationship used in this study (**Panel A**). The corresponding stroke volume – cardiac output relationship is shown in **Panel B**. This relationship is based on linear interpolation of data recorded in healthy adults from WF Boron and EL Boulpaep, *Medical Physiology*, Elsevier Science 2003.

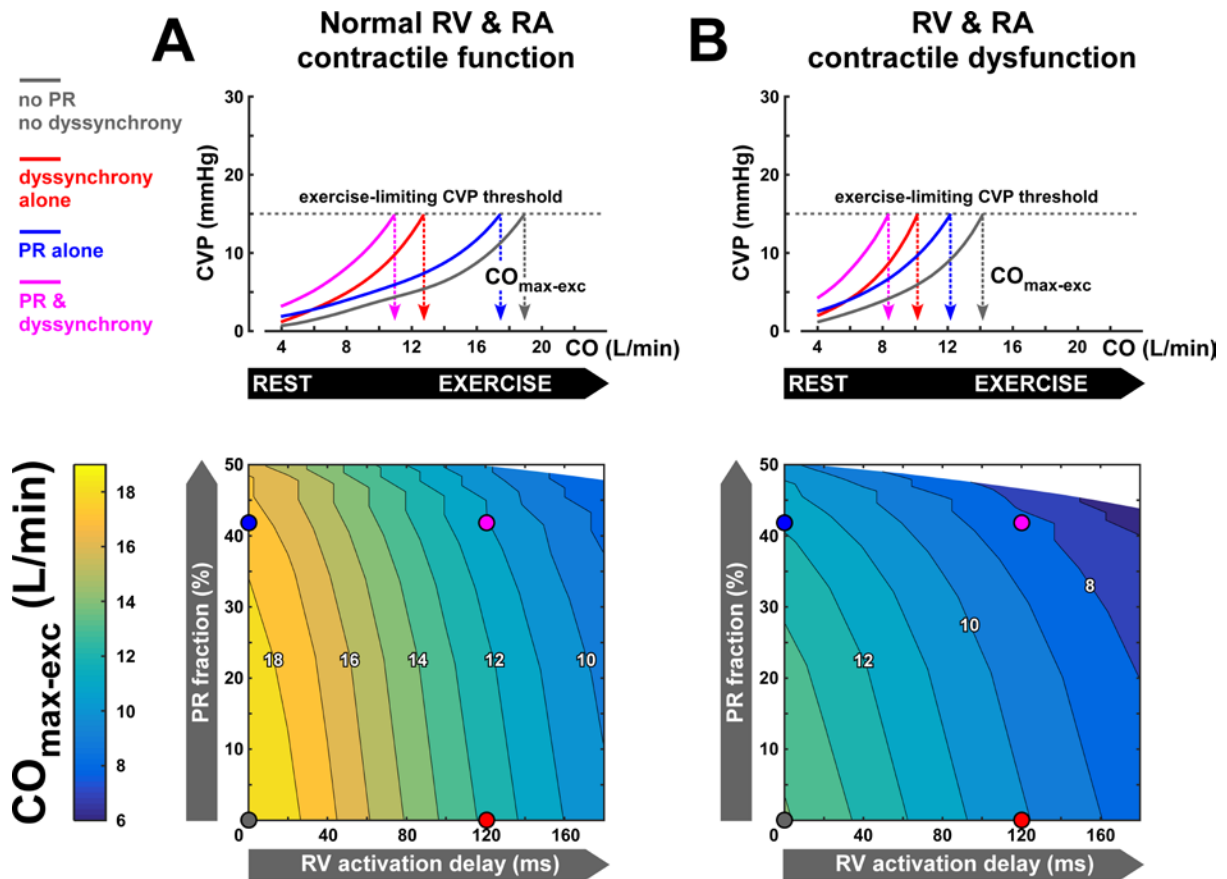


**Figure S4:** Exercise capacity (using 15 mmHg as the pressure threshold) as function of right ventricular (RV) dyssynchrony and pulmonary regurgitation (PR) in the virtual rTOF patient cohorts with normal (**panel A**) and decreased (**panel B**) contractile function of the RV and right atrial (RA) myocardium. The upper panels show how CVP rises with CO during exercise in four representative virtual rTOF patients. Those virtual patients are marked by circles in the heat plots showing continuous effects of RV dyssynchrony and PR on exercise capacity. Simulated exercise capacity is defined as the virtual patient's cardiac output ( $CO_{\max\text{-exc}}$ ) associated with the exercise-limiting central venous pressure (CVP) threshold. In general, RV dyssynchrony and contractile dysfunction are more limiting for exercise capacity than PR.

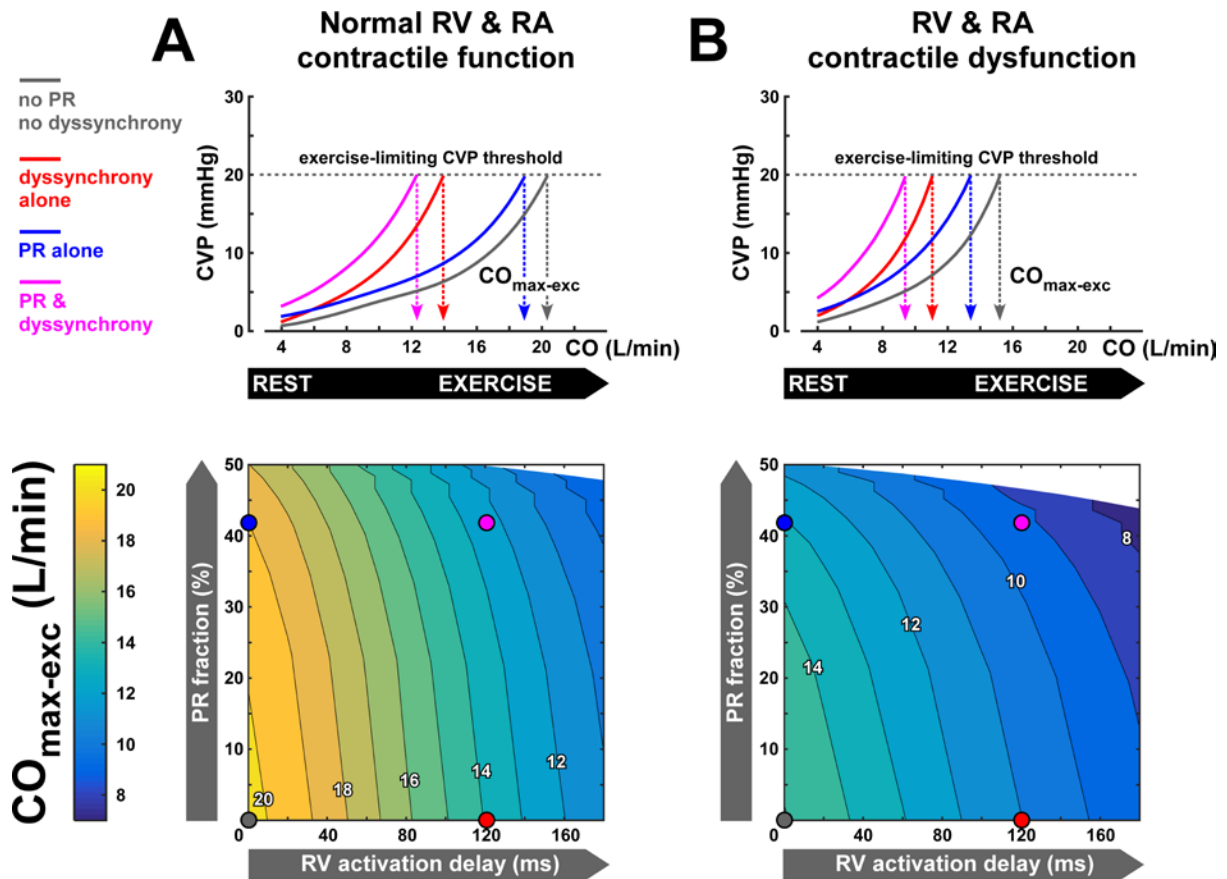


**Figure S5:** Exercise capacity (using 20 mmHg as the pressure threshold) as function of right ventricular (RV) dyssynchrony and pulmonary regurgitation (PR) in the virtual rTOF patient cohorts with normal (**panel A**) and decreased (**panel B**) contractile function of the RV and right atrial (RA) myocardium. The upper panels show how CVP rises with CO during exercise in four representative virtual rTOF patients. Those virtual patients are marked by circles in the heat plots showing continuous effects of RV dyssynchrony and PR on exercise capacity. Simulated exercise capacity is defined as the virtual patient's cardiac output ( $CO_{max-exc}$ ) associated with the exercise-limiting central venous pressure (CVP) threshold. In general, RV dyssynchrony and contractile dysfunction are more limiting for exercise capacity than PR.